

Dissecting the IRX – β dust attenuation relation: exploring the physical origin of observed variations in galaxies

Gergő Popping^{1*}, Annagrazia Puglisi^{1,2}, and Colin A. Norman^{3,4}

¹*European Southern Observatory, Karl-Schwarzschild-Strasse 2, 85748, Garching, Germany*

²*Dipartimento di Fisica e Astronomia, Università di Padova, vicolo dell’Osservatorio 2, I-35122 Padova, Italy*

³*Department of Physics and Astronomy, Johns Hopkins University, Baltimore, MD 21218, USA*

⁴*Space Telescope Science Institute, 3700 San Martin Drive, Baltimore, MD 21218, USA*

September 3, 2021

ABSTRACT

The use of ultraviolet (UV) emission as a tracer of galaxy star-formation rate (SFR) is hampered by dust obscuration. The empirical relationship between UV slope, β , and the ratio between far-infrared and UV luminosity, IRX, is commonly employed to account for obscured UV emission. We present a simple model that explores the physical origin of variations in the IRX – β dust attenuation relation. A relative increase in FUV compared to NUV attenuation and an increasing stellar population age cause variations towards red UV slopes for a fixed IRX. Dust geometry effects (turbulence, dust screen with holes, mixing of stars within the dust screen, two-component dust model) cause variations towards blue UV slopes. Poor photometric sampling of the UV spectrum causes additional observational variations. We provide an analytic approximation for the IRX – β relation invoking a subset of the explored physical processes (dust type, stellar population age, turbulence). We discuss observed variations in the IRX – β relation for local (sub-galactic scales) and high-redshift (normal and dusty star-forming galaxies, galaxies during the epoch of reionization) galaxies in the context of the physical processes explored in our model. High spatial resolution imaging of the UV and sub-mm emission of galaxies can constrain the IRX – β dust attenuation relation for different galaxy types at different epochs, where different processes causing variations may dominate. These constraints will allow the use of the IRX – β relation to estimate intrinsic SFRs of galaxies, despite the lack of a universal relation.

Key words: ISM: dust, extinction – galaxies: ISM – galaxies:high redshift – ultraviolet: galaxies – infrared: galaxies

1 INTRODUCTION

A reliable measurement of the star-formation rate (SFR) of galaxies is a key component of our understanding of galaxy formation and evolution. A commonly used approach to measure the SFR of galaxies accounts for the ultraviolet emission from short-lived massive stars (Kennicutt & Evans 2012). This approach is especially popular for high-redshift galaxies up to redshifts of $z \sim 10$, where broadband UV photometry is available through deep field studies (e.g., Bouwens et al. 2011; Dunlop et al. 2012; Ellis et al. 2013; Oesch et al. 2014, 2015; Bouwens et al. 2015; McLeod et al. 2015). The use of UV as a SFR tracer is hampered by the absorption of UV radiation by dust in the interstel-

lar medium (ISM). The absorbed radiation is re-emitted in the infrared (IR), and ideally far-IR measurements complementary to UV detections are available to account for the absorbed emission. Unfortunately, especially at $z > 3$ IR information is not always available due to various reasons (e.g., detection limits and source confusion in *Spitzer Space Telescope* and *Herschel Space Observatory* bands) and alternative approaches to account for the absorbed UV emission have to be used.

A commonly used approach to account for the absorbed UV emission is the empirical relation between the rest-frame UV continuum slope β (where $F_\lambda \propto \lambda^\beta$) and the ratio between the infrared and UV luminosity (IRX) in local (blue starburst) galaxies (Calzetti 1997; Meurer, Heckman & Calzetti 1999; Overzier et al. 2011; Takeuchi et al. 2012). This relation correlates the UV slope to dust extinction,

* E-mail: gpopping@eso.org

which then is used to correct the UV photometry for dust obscuration and derive the intrinsic (dust-obscured plus unobscured) SFR of galaxies. If the scatter in this relation is minimal over a range of galaxy types over cosmic time, it can serve as a straightforward way to infer the intrinsic SFR of galaxies when only UV measurements are available. The IRX – β relation has been widely used to estimate the intrinsic SFR in high-redshift galaxies for which IR data is not available (e.g., Bouwens et al. 2011; Ellis et al. 2013; Oesch et al. 2014, 2015; Bouwens et al. 2015; McLeod et al. 2015). Accounting for dust obscured star formation at high redshifts is essential, as observations and models suggest that galaxies at $z > 7$ can already have significant reservoirs of dust (e.g., Watson et al. 2015; Popping, Somerville & Galametz 2016; Laporte et al. 2017; Strandet et al. 2017). The use of the IRX – β relation for high-redshift galaxies is supported by observations that showed that the Meurer et al. IRX – β relation is broadly appropriate for samples of main-sequence galaxies at $z \sim 2 - 4$ (Reddy et al. 2008; Pannella et al. 2009; Reddy et al. 2010, 2012; Heinis et al. 2013; To, Wang & Owen 2014; Coppin et al. 2015; Álvarez-Márquez et al. 2016; Puglisi et al. 2016; Bourne et al. 2017; Fudamoto et al. 2017).

Despite its promising nature, local and high-redshift studies have showed that some galaxies deviate from the IRX – β relation. Nearby ultra-luminous infrared galaxies (ULIRGS) have large values of IRX with a low value of β , corresponding to a blue UV continuum slope (Goldader et al. 2002). Observations of ordinary spiral galaxies in the local Universe showed larger values for β (corresponding to a redder UV continuum slope) for a given IRX compared to the Meurer, Heckman & Calzetti (1999) relation (Kong et al. 2004; Buat et al. 2005; Grasha et al. 2013). The latter was explained by older and less massive stars contributing to the near-UV emission of galaxies. Metal poor systems such as the Magellanic clouds have redder colours than metal-rich systems (Bell et al. 2002; Bell 2002). There are many other works that have explored variations in the IRX – β relation and their physical cause in local galaxies (e.g., Burgarella, Buat & Iglesias-Páramo 2005; Seibert et al. 2005; Cortese et al. 2006; Gil de Paz et al. 2007; Johnson et al. 2007; Panuzzo et al. 2007; Cortese et al. 2008; Siana et al. 2008; Boquien et al. 2009; Muñoz-Mateos et al. 2009; Wijesinghe et al. 2011; Boquien et al. 2012; Ye et al. 2016). High-redshift observations have demonstrated that dusty star-forming galaxies (DSFGs) have bluer UV continuum slopes for a given IRX (increasingly deviating from the Meurer et al. relation as a function of IR luminosity, e.g., Oteo et al. 2013; Casey et al. 2014; Bourne et al. 2017). High-redshift Lyman Break Galaxies are observed to have redder UV continuum slopes β for a given IRX value, more consistent with a Small Magellanic Cloud (SMC) or Large Magellanic Cloud (LMC) attenuation curve than the canonical Meurer, Heckman & Calzetti (1999) relation (e.g., Capak et al. 2015; Bouwens et al. 2016; Koprowski et al. 2016; Pope et al. 2017; Smit et al. 2017). A similar conclusion was reached for normal star-forming galaxies at $z \sim 2$ (Reddy et al. 2012, 2017) and for lensed Lyman Break Galaxies at $z \sim 3$ (Siana et al. 2008, 2009). Recently, Fudamoto et al. (2017) found that IRX decreases as a function of look-back time for normal star-forming galaxies at $z \sim 4 - 6$ at a given UV slope β .

A reliable use of the IRX – β relation to estimate the dust-obscured star formation (SF) in galaxies requires a detailed understanding of the physical origin of the aforementioned variations. Multiple theoretical efforts have addressed the origin of observed variations in the IRX – β relation (e.g., Granato et al. 2000; Ferrara et al. 2016; Mancini et al. 2016; Cullen et al. 2017; Narayanan et al. 2017; Safarzadeh, Hayward & Ferguson 2017). These works have highlighted stellar population age, variations in the dust attenuation curve, the temperature of the dust, and the geometry of the dust distribution as possible origins for observed deviations from the Meurer et al. IRX – β relation.

In this work we present a simple model to systematically explore how different properties of the stellar population (age), different properties of the absorbing dust screen (dust attenuation curve, turbulence, geometry, mixing of stars and dust, and a two-component dust model), and observational effects affect the IRX – β relation of galaxies. We present our methodology in Section 2 and a detailed analysis of the physical origin of variations in the IRX – β relation in Section 3. We discuss our results in Section 4, focusing on the physical origin of the IRX – β relation, observed variations in the IRX – β relation in the context of our model results, an analytic approximation of the IRX – β relation, and a future outlook towards reliably using the IRX – β relation as a tracer of dust-obscured star-formation. We summarise our results in Section 5.

2 MODEL DESCRIPTION

In this work we use a simple model in which we place a screen of dust in front of a single burst simple stellar population. Throughout the paper we vary the properties of the screen and the properties of the stellar population.

2.1 Stellar population model

We use the `Starburst99` (Leitherer et al. 1999) simple stellar population model to create stellar spectra. The Spectral Energy Distributions (SEDs) are calculated as simple stellar population models with a fixed stellar mass at different ages and metallicities. The model assumes a Kroupa (2002) initial mass function and the Geneva Isochrones without rotation (Ekström et al. 2012; Georgy et al. 2013). Unless noted differently we use an SED generated assuming a stellar age of 10 Myr and solar metallicity.

2.2 Dust screen

The attenuation by dust is modelled using the attenuation curves from Seon & Draine (2016). Seon & Draine apply radiative transfer models in a spherical, clumpy interstellar medium to investigate the attenuation of starlight. In this model the turbulent dusty medium and stellar sources are spherically distributed within a radius of R_d and R_s for dust and stars, respectively. Photon sources are uniformly distributed within the stellar sphere. The radial extent of the stellar sources is varied within the range $0 < R_s/R_d < 1$. $R_s/R_d = 1$ corresponds to a case where the photon sources are uniformly distributed over the dusty sphere (photon

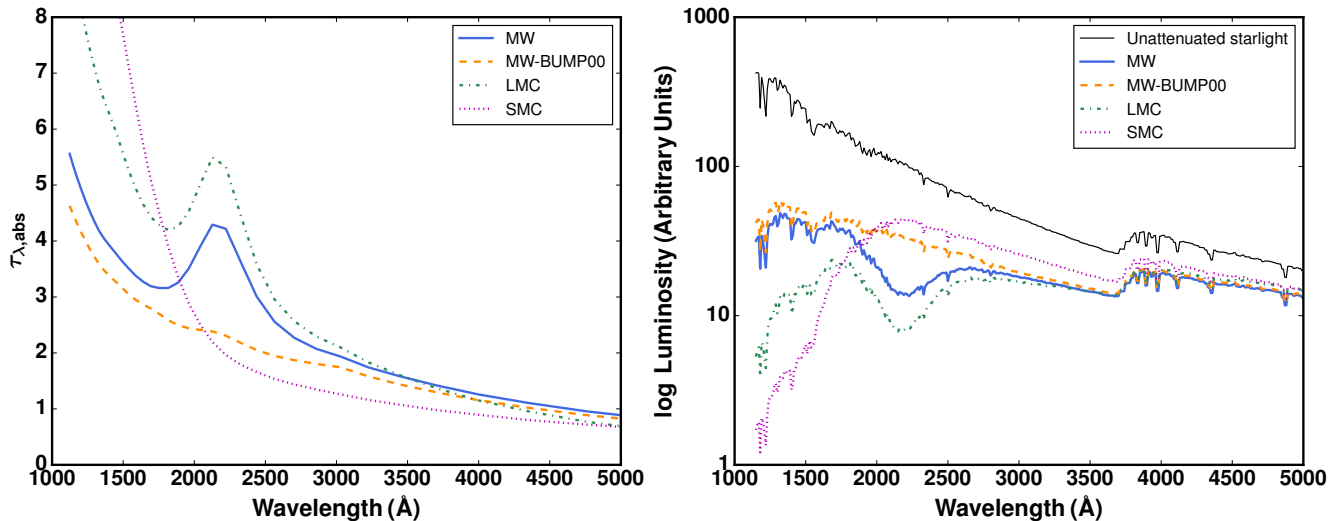


Figure 1. Left: The dust extinction curves applied in this work for a mean homogeneous optical depth in the V band of one ($\langle \tau_V \rangle = 1$) and assuming a uniform medium ($\mathcal{M} = 0$) and $R_s/R_d = 0$. Right: The unobscured (black) and obscured (coloured) stellar emission spectra of a single burst population with an age of 10 Myr and solar metallicity. The obscured spectra are based on the attenuation curves shown in the left panel.

sources are uniformly mixed), whereas $R_s/R_d = 0$ corresponds to a medium where the photon sources are surrounded by a dusty cloud (Seon & Draine 2016). The latter case can be seen as a screen of dust located between the photon sources and the observer. We point the reader to Figure 4 in Seon & Draine (2016) for a schematic representation of the spatial distribution between dust and photon sources.

The Seon & Draine model provides attenuation optical depths due to absorption and scattering from approximately 1000 Å to 3 μm , as a function of mean homogeneous V-band optical depth ($\langle \tau_V \rangle$; from $\langle \tau_V \rangle = 0.1$ to $\langle \tau_V \rangle = 20$). Seon & Draine (2016) define the homogeneous V-band optical depth as the centre-to-edge optical depth of a cloud with a constant density and radius R_d . Photon packages that escape the spherical dust cloud are recorded as f_λ^{esc} as a function of wavelength. Depending on the optical depth of the system, between 10^5 and 10^7 photon packages are used for each wavelength. The attenuation optical depth is then calculated as $\tau_\lambda^{\text{att}} = -\ln(f_\lambda^{\text{esc}})$. The attenuation optical depth in the V-band is often less than the homogeneous V-band optical depth, as a significant fraction of the scattered light does escape the dust sphere towards the observer. In this work we adopt attenuation curves based on the following dust types from Weingartner & Draine (2001): Milky Way (MW), Milky Way without the 2175 Å bump (MW-BUMP00), Large Magellanic Cloud (LMC), and Small Magellanic Cloud (SMC).

The Seon & Draine (2016) model takes the turbulence of the screen of dust into account. When no turbulence is present the screen has a uniform distribution of dust and the optical depth seen by the stellar light is identical at any point on the screen surface. Under the influence of turbulence the mean optical depth in the V-band $\langle \tau_V \rangle$ of a screen of dust stays the same, but locally the optical depth increases or decreases (see also for example Fischera, Dopita & Sutherland 2003; Fischera & Dopita 2005). This naturally adds geometry to the screen of dust and changes the attenuation properties. The Seon & Draine (2016) model explores the

level of turbulence of the dust screen from a uniform screen (Mach number $\mathcal{M} = 0$) to a highly turbulent screen (Mach number $\mathcal{M} = 20$). We interpolate between wavelength λ , mean V-band optical depth, R_d/R_s , and Mach number to derive optical depths as a function of the aforementioned properties.

The attenuated stellar emission at any wavelength, mean V-band optical depth, Mach number, and R_d/R_s is given as

$$I_{*,\text{att}}(\lambda, \langle \tau_V \rangle, \mathcal{M}, R_d/R_s) = I_*(\lambda) \times e^{-\tau^{\text{att}}(\lambda, \langle \tau_V \rangle, \mathcal{M}, R_d/R_s)}, \quad (1)$$

where $I_*(\lambda)$ is the unattenuated stellar emission.

As an example we show the attenuation curve for the MW, MW-BUMP00, LMC, and SMC in the left panel of Figure 1 (assuming $\langle \tau_V \rangle = 1$, $\mathcal{M} = 0$, and $R_d/R_s = 0$). There are clear differences between the attenuation curves, especially in the level of attenuation at UV wavelengths (up to ~ 3000 Å). Besides the presence of the 2175 Å bump in the MW and LMC curves, the LMC and SMC curves show much more attenuation in the FUV regime. The LMC curve shows an elevated level of attenuation compared with the MW curves at wavelengths $\lambda < 4500$ Å, whereas the SMC curve has an elevated level of attenuation at wavelengths $\lambda < 2000$ Å. The right panel of Figure 1 shows the unattenuated stellar emission of a single burst population with solar metallicity and an age of 10 Myr, and the attenuated spectra for the MW, MW-BUMP00, LMC, and SMC attenuation curves presented in the left panel of Figure 1. The 2175 Å feature is clearly visible in the attenuated spectra for the MW and LMC attenuation curves. The strong increase in absorption for the SMC attenuation curve at wavelengths less than 2000 Å reflects itself by a steeply rising attenuated stellar emission in the same wavelength range.

Unless noted differently, we use a uniform dust screen ($\mathcal{M} = 0$) with $R_d/R_s = 0$ in the remaining of the paper. In this work we always assume a single burst stellar population,

rather than the more realistic composite stellar populations galaxies consist of.

2.3 Calculating β & IRX

The UV-slope β is computed assuming that the (attenuated) stellar emission can be described by a power-law between wavelength and flux, with $F_\lambda \propto \lambda^\beta$. The UV-slope β is approximated by a log-linear fit in the wavelength range 1230 – 3200 Å. This wavelength range corresponds to UV radiation from O and B stars and ensures a broad wavelength coverage around the 2175 Å feature, if present.

The infrared excess (IRX) is computed as

$$\text{IRX} = \frac{L_{\text{IR}}}{L_{1600\text{Å}}}, \quad (2)$$

where $L_{1600\text{Å}}$ is the UV luminosity at 1600 Å and L_{IR} is the infrared luminosity. We assume that all absorbed stellar emission L_{abs} is re-emitted in the infrared, which gives an infrared luminosity of $L_{\text{IR}} = L_{\text{abs}}$.

3 RESULTS

In this Section we vary the properties of the stellar population and the screen of dust to explore how such variations change the IRX – β relation of dust attenuation. We will vary the stellar age and dust attenuation curve (Sec. 3.1), introduce turbulence in the dust screen (Sec. 3.2), vary the covering fraction of the dust screen (Sec. 3.3), mix the stars in between the dust (Sec. 3.4.1), introduce a two-component dust model (Charlot & Fall 2000, Sec. 3.4.2), and explore how observational effects change the measured IRX – β relation (3.5). Throughout this section we compare our results to four IRX – β relations from the literature: The seminal Meurer, Heckman & Calzetti (1999) relation for local starburst;¹ a refit to the galaxies in (Meurer, Heckman & Calzetti 1999) by Overzier et al. (2011) based on *Galaxy Evolution Explorer* (*GALEX*) data; a fit by Casey et al. (2014) to local galaxies covering a large range in SFRs; and the IRX – β relation for SMC dust based on Pettini et al. (1998).

3.1 Varying dust type and stellar population age

We show the IRX – β relation for the four different types of dust attenuation curves explored in this work (MW, MW-BUMP00, LMC, and SMC) for stellar populations with ages running from 1 to 100 Myr in Figure 2. The SMC relation is flatter than the MW relation, with the LMC relation lying in between. Due to the elevated level of attenuation in the UV regime for the SMC and LMC attenuation curves (see Figure 1), the slope β will be steeper compared to MW dust types. As the optical depth of the dust slab increases, the FUV emission is relatively more absorbed than the NUV.

¹ The Meurer, Heckman & Calzetti (1999) IRX – β relation is based on a FIR luminosity covering the wavelength range 40–120 μm , rather than the entire IR wavelength regime. Meurer, Heckman & Calzetti (1999) find that these are typically different by a factor of ~ 1.4 .

This moves the IRX – β relation to the right compared to the MW type attenuation curves and causes the flattening in the IRX – β relation from MW to SMC dust types. These results immediately demonstrate that simply by changing the dust-type the relation between UV-slope and infrared excess can change significantly. There is hardly any difference between the MW and MW-BUMP00 IRX – β relation, which suggests that the effect of the 2175 Å on the location of galaxies in the IRX – β plane is minimal.²

There is a clear trend in the IRX – β relation as a function of the age of the stellar populations. With age, the UV part of a stellar spectrum becomes redder, naturally shifting the IRX – β relation to higher values of the UV-slope β .

The simple model presented in this work reproduces the observed relations very well. The shapes of the theoretical IRX – β relation are similar to the observed relations. The MW models for a stellar population with an age of 10 Myr are very close to the Casey et al. (2014) fit to local galaxies. The Meurer, Heckman & Calzetti (1999) and Overzier et al. (2011) fit to local starbursts it typically located above our model results (except for populations with ages of ~ 1 Myr). The LMC and SMC curves for a population of 10 Myr are both close to the IRX – β relation for SMC dust in the literature (Pettini et al. 1998). The match between our predicted and the observed IRX – β relations suggests that the observed relations are consistent with a simple screens of dust in front of a relatively young population of stars.

3.2 A turbulent sheet of dust

A small level of turbulence within a dust screen can locally increase or decrease the column of dust the stellar emission has to travel through. This turbulence can for instance be caused by shocks or shear motions within spiral arms. Although the volume weighted mean optical depth due to absorption remains the same, locally the optical depth varies. Because the absorption of light scales exponentially with optical depth, the net amount of light passing through the screen of dust will vary. This was initially explored by Fischera, Dopita & Sutherland (2003), who showed that with an increasing level of turbulence more light passes through a screen of dust. The authors found that turbulence drives dense clumps of dust with high optical depth where no light passes through. This is balanced by large areas with low optical depth where almost all the stellar emission passes through. This was explored further by Seon & Draine (2016) who reached similar conclusions and demonstrated that the shape of the net attenuation curve (by averaging over all the sight lines) changes with increasing level of turbulence. A change in shape of the attenuation curve will naturally affect the UV-slope β and IRX.

We show how β and IRX change as a function of $\langle \tau_V \rangle$ and Mach number in Figure 3. Both β and IRX decrease when the level of turbulence increases. IRX decreases due to the overall level of absorption decreasing. The UV emission escaping the dust screen is dominated by emission from

² We will show in Section 3.5 that the 2175 Å bump can contaminate a poor photometric sampling of the UV spectra of galaxies and affect the reconstructed IRX – β relation.

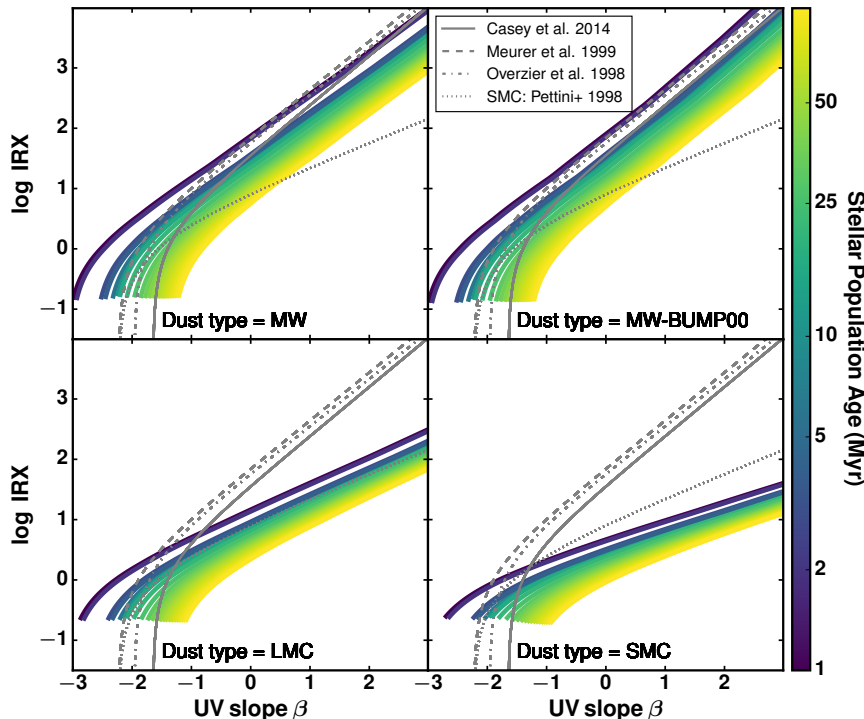


Figure 2. The IRX – β relation for different dust types and a varying age of the stellar population compared to observed IRX – β relations (Meurer, Heckman & Calzetti 1999; Overzier et al. 2011; Casey et al. 2014; Pettini et al. 1998). Larger values of IRX correspond to an increased optical depth. Older populations shift the relation to larger values of UV-slope β . An increased FUV attenuation component (LMC and SMC dust types) flattens the IRX – β relation.

regions with low optical depth. In these regions the attenuated stellar emission is closer to the original unattenuated spectrum than for a homogeneous screen of dust. This naturally decreases the UV-slope β . The same trend occurs for the four different dust types.

We show the IRX – β relation for varying levels of turbulence in Figure 4. The IRX – β relation shifts above the relation for a homogeneous dust screen with increasing level of turbulence. This effect is stronger for MW dust types than for LMC and SMC types of dust. In other words, this effect becomes less important for attenuation curves with a strong FUV component. The scatter in IRX increases as a function of UV slope β .

3.3 The covering fraction of the dust

In the previous Section we explored the effects of turbulence within the dust screen on the IRX – β relation, where turbulence led to a locally elevated or decreased optical depth. A more extreme version of this is a patchy screen, i.e. a screen with holes in it. If the screen is patchy and thus has a dust covering fraction less than one (the screen has holes), some fraction of the stellar emission can escape the screen without ever being absorbed or scattered.

In Figure 5 we show how UV-slope β and IRX evolve as a function of mean homogeneous optical depth in the V-band of the dust screen and the fraction of non-obscured emission (i.e. the fraction of emission not passing through a dust screen). A non-obscured fraction of zero means that all of the stellar emission passes through a dust screen, whereas

a non-obscured fraction of one means that none of the emission passes through a dust screen (in other words, there is no screen of dust between the photon source and the observer). We find that both the UV-slope β and the infrared excess IRX decrease with an increased fraction of non-obscured emission. When less emission is obscured, the fraction of absorbed emission automatically decreases, which yields lower values of IRX. Similarly, the UV emission from the non-obscured regime will dominate over the UV emission from the obscured regime, resulting into a lower value for β . Interestingly, when a non-obscured component is present the UV-slope β increases and then decreases again as a function of mean homogeneous optical depth. The turning point marks the mean homogeneous optical depth where UV emission from the non-obscured regions starts to dominate over the UV emission from the obscured regions. IRX remains almost constant once the optical depth is larger than the optical depth corresponding to the turning point in β . At these optical depths the slab of dust is so optically thick that effectively all the stellar emission is absorbed and re-emitted in the IR. From this point on, the IR luminosity thus remains almost constant as the optical depth increases. The UV emission is completely dominated by the UV emission from the non-obscured region, and also remains constant. This results in a constant value for IRX. It is worth noting that if the non-obscured fraction of the stellar emission is very small, the UV emission escaping the system may be too faint to observe.

We show the IRX – β relation as a function of non-obscured fraction for four different dust types in Figure 6.

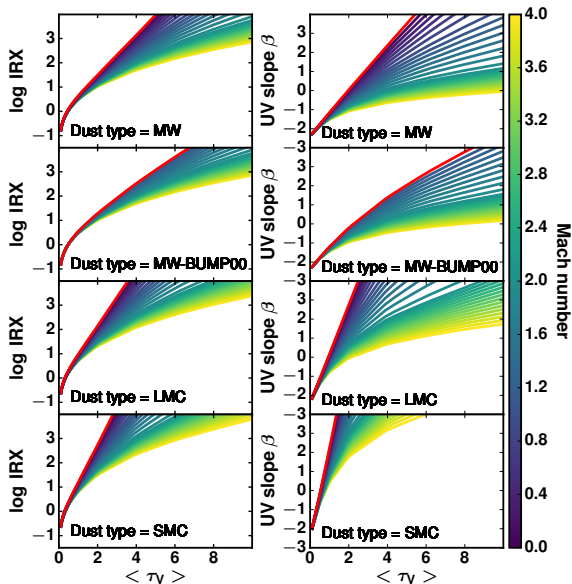


Figure 3. The UV-slope β and infrared excess (IRX) as a function of mean homogeneous optical depth in the V-band and Mach number for different types of dust attenuation curves. The red lines show β and IRX for a dust screen without turbulence (i.e., $\mathcal{M} = 0$). As the level of turbulence increases, both β and IRX decrease.

When a non-obscured component is present, the IRX – β relation first follows the relation for a dust screen completely obscuring the stellar emission. However, the relation then turns backwards towards lower values of β while still increasing IRX. As before, the turning points marks the mean homogeneous optical depth where UV emission from non-obscured regions starts to dominate over the UV emission from obscured regions (Figure 5). A very low non-obscured fraction (less than 1%) in combination with a large optical depth result in a scatter in IRX up to 2–3 dex for a given UV slope β .

3.4 Mixing of stars and dust

3.4.1 Mixing of stars and dust within a birth-cloud

We have so far assumed that the screen of dust is located between the stars and the observer (i.e., $R_d/R_s = 0$). We will now explore the effects of mixing stars with the dust (varying R_d/R_s) on the IRX – β relation in Figure 7. The IRX – β relation shifts towards higher values of IRX and lower values for UV-slope β with increasing R_d/R_s . As R_d/R_s increases, some of the stars will see a smaller column of dust (since they are located towards the edge of the screen of dust facing the observer). As a result, the total absorption of starlight and consequently IRX both decrease. Because some of the stars are less attenuated the spectrum will also remain bluer, decreasing the UV-slope β . This effect is strongest for a homogeneous mixing of dust and stars ($R_d/R_s = 1$). For this scenario there will always be stars whose emission is not attenuated at all, which rapidly results in lower values for IRX and β .

3.4.2 Dusty birth clouds within a diffuse dusty ISM

A more realistic representation of the mixing of stars and dust is the two-component model put forward by Charlot & Fall (2000). In this model the birth clouds of stars are homogeneously distributed within a diffuse dusty ISM. To represent this we assume that the emission from stars is exposed to two screens of dust. First, a screen of dust with $R_d/R_s = 0$, representing the birth cloud surrounding the young stars. The attenuated stellar emission that escapes the first screen passes through a second dust screen with $R_d/R_s = 1$. This means that the birth clouds are homogeneously distributed within a second screen of dust representing the diffuse dusty ISM. The resulting IRX – β relations are presented in Figure 8. The colour coding in this Figure corresponds to fixed optical depths for the screen of dust representing the diffuse dusty ISM. An increase in IRX along a line with fixed colour corresponds to an increase in the optical depth of the screen representing the birth clouds.

The IRX – β relation moves towards bluer UV colours β at fixed IRX as the optical depth in the screen of dust representing the diffuse dusty ISM increases. This is driven by variations in optical depth seen by the stellar emission that escapes the birth clouds. For some of the birth clouds the emission that reaches the observer had to travel through the entire slab representing the diffuse dusty ISM. The stellar emission is further absorbed and contributes to the infrared emission (and thus drives IRX to higher values). Other birth clouds will be located at the observer side of the slab of dust representing the diffuse dusty ISM. For these clouds the escaped stellar emission (almost) directly travels to the observer without additional absorption. This emission is the dominant source of the UV emission that reaches the observer and will control the UV slope β . While IRX is weighted towards stellar emission that is further absorbed, β is weighted towards stellar emission that is not further absorbed. As a result, β is relatively blue for a given IRX.

As becomes apparent from Figure 8, an increase in $\langle \tau_V \rangle$ for the screen of dust representing the diffuse dusty ISM results in a minimum value for the UV slope β . This minimum represents the scenario where the optical depth of the birth cloud equals zero (the stars are not located within birth clouds anymore). For this scenario the two-component model is identical to the scenario explored in Section 3.4.1 with $R_s/R_d = 1$.

Changes in the IRX – β relation due to the two-component model become significant when the diffuse dusty ISM has a homogeneous mean optical depth of $\langle \tau_V \rangle \sim 4$, or higher. These environments should only be relevant for relatively dust-rich systems such as DSFGs.

3.5 Deviations from IRX – β relation due to observational effects

Up to this point the UV-slope β was calculated by a fit to the attenuated stellar spectrum. Unfortunately, observations are often limited to photometric datapoints (especially at high redshifts) and β is then computed based on a fit to photometric sampling of the UV emission (e.g., Casey et al. 2014; Capak et al. 2015; Puglisi et al. 2016; Smit et al. 2016; Reddy et al. 2017). The 1600 Å UV luminosity that enters the IRX

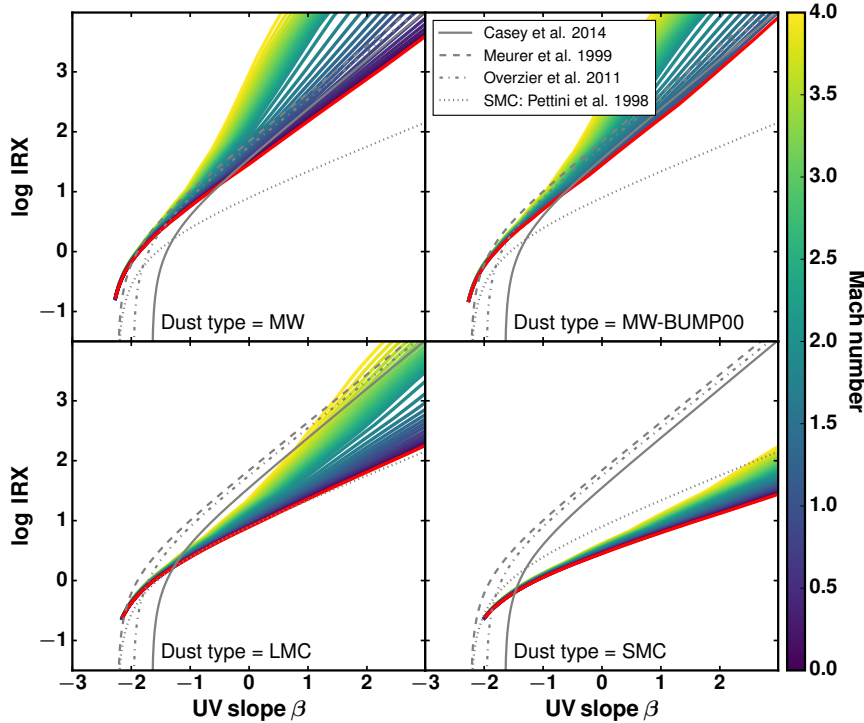


Figure 4. The IRX – β relation for varying levels of turbulence within the screen of dust. The relations are plotted for different dust types. The red lines show the IRX – β relation for a dust screen without turbulence (i.e., $\mathcal{M} = 0$). Turbulence within the dust screen can significantly alter the location of a galaxy within the IRX – β plane.

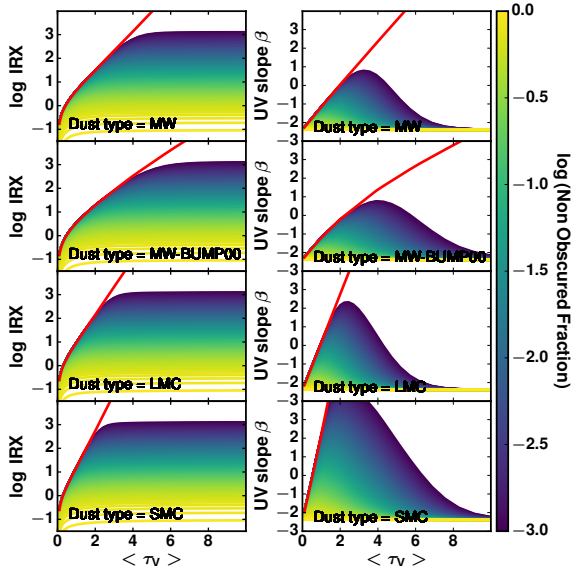


Figure 5. The UV-slope β and infrared excess (IRX) as a function of mean homogeneous optical depth in the V-band and the obscuration fraction of the stellar emission for different dust attenuation curves. The red lines show β and IRX for a dust screen with a non-obscured fraction of zero (i.e., all the emission passes through a dust screen). As the non-obscured fraction increases, both β and IRX decrease. Most intriguingly, a small non-obscured fraction can already lead to blue UV-slopes for high-values of $\langle \tau_V \rangle$.

calculations is estimated by an interpolation between the photometric datapoints. To mimic this, in this Section we calculate the UV-slope β and 1600 Å UV luminosity based on a fit to photometric datapoints of the attenuated stellar emission from $z = 0$ to $z = 8$. Photometric datapoints were obtained by convolving the redshifted attenuated stellar light with telescope filters probing the rest-frame UV wavelength range ($1230 < \lambda < 3200\text{Å}$). Depending on the redshift of interest and combination of filters, the UV-slope β is calculated based on 2 up to 6 (or even more) photometric datapoints.

Figure 9 gives an example of the coverage of the UV rest-frame wavelength regime by different filters at different redshifts. We use the same set of filters that were used for the 3D-HST survey (Skelton et al. 2014), combined with *GALEX*, and a Ks-band filter. This Figure immediately demonstrates that in some cases the power-law fit to the photometric datapoints may suffer from a poor sampling of strong FUV absorption (for example at $z = 1$ for an SMC dust attenuation curve) or a contamination of the fit by the 2175 Å bump (for example at $z = 0$, $z = 1$, and $z = 8$).³ A poor sampling or contamination can result in a poor estimation of the UV-slope β and the UV luminosity, introducing a systematic error in the IRX – β relation (Kriek & Conroy 2013).⁴

³ Observational constraints on the 2175 Å bump indicate that this bump is typically not as strong in extragalactic sources as in our own Galaxy (e.g., Kriek & Conroy 2013)

⁴ Besides a poor fit to the rest-frame UV wavelength regime, additional uncertainty may be introduced when estimating the

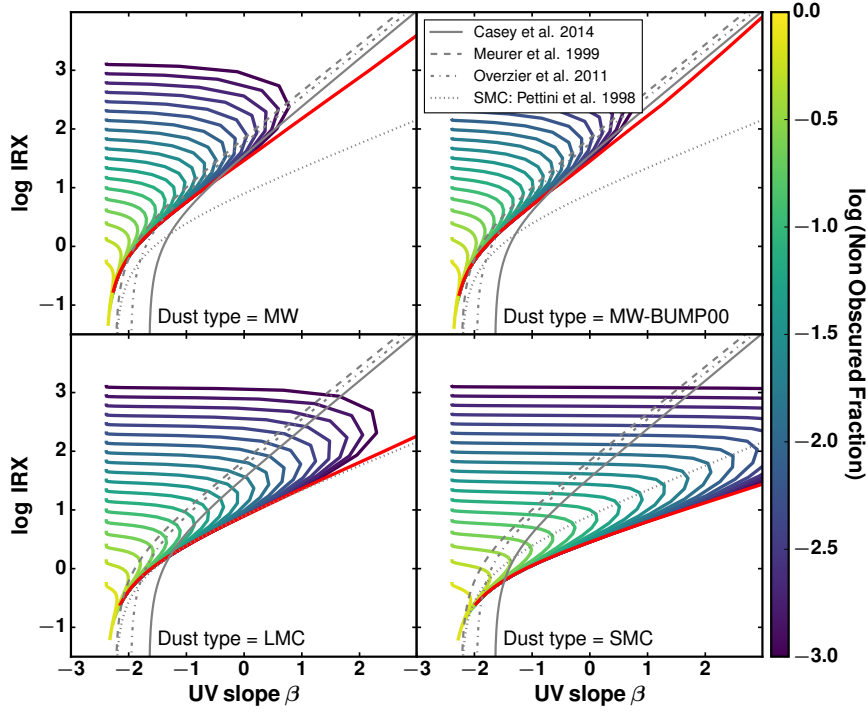


Figure 6. The IRX – β relation when a fraction of the stellar light is not obscured. The relations are plotted for different dust types. The red lines show the IRX – β relation for a dust screen with an non-obscured fraction of zero (i.e., all the emission passes through a dust screen). A small fraction of non-obscured emission can completely alter the location of a galaxy within the IRX – β plane, with high IRX and blue UV-slope β .

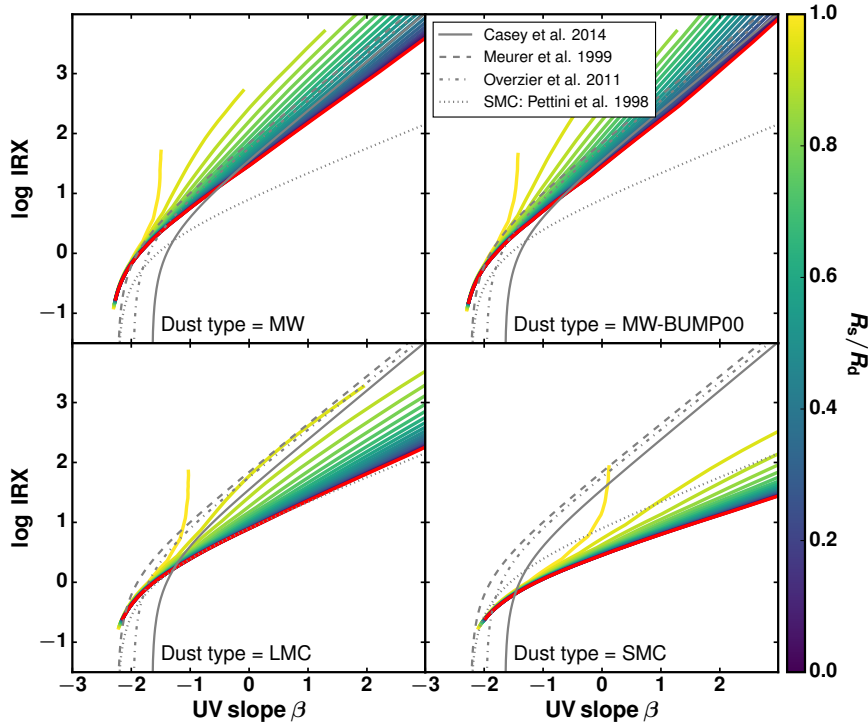


Figure 7. The IRX – β relation when the young stars are distributed within the dust screen (rather than placed before the dust screen). The relations are plotted for different dust types. The red lines show the IRX – β relation for the scenario where $R_s/R_d = 0$ (i.e., the dust screen is located between the stars and the observer). Mixing the stars between the dust lowers IRX values, makes the attenuated spectra bluer, and causes offsets above the $R_s/R_d = 0$ IRX – β relation.

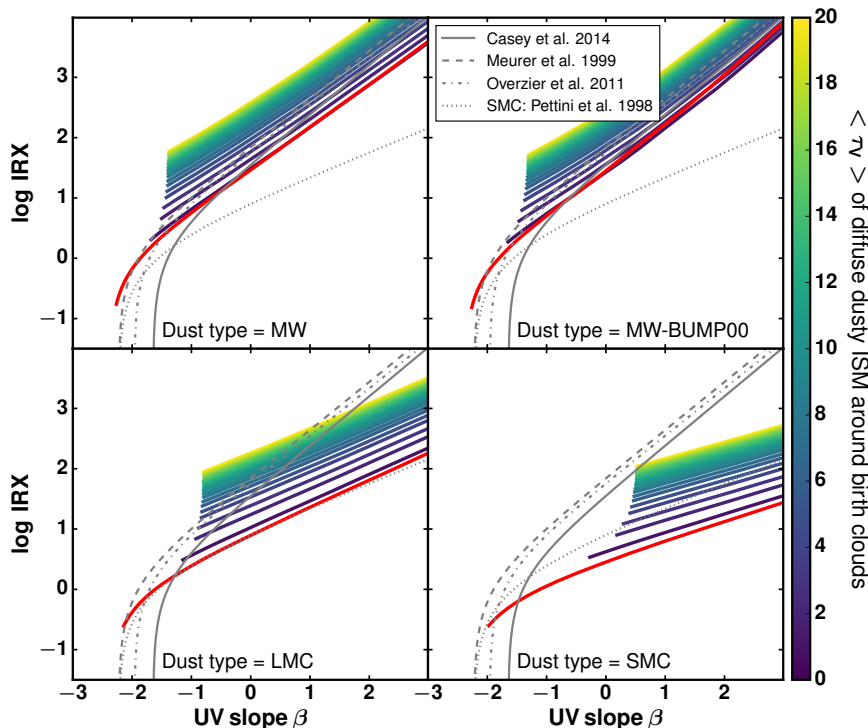


Figure 8. The IRX - β relation when we assume that birth clouds are homogeneously distributed within a diffuse dusty ISM (two-component dust model; Charlot & Fall 2000). The stellar emission passes through two screens. First a screen with $R_s/R_d = 0$, representing the birth clouds of stars. The second screen representing the diffuse dusty ISM has $R_s/R_d = 1$, a homogeneous mixing of photon sources (the emission escaping from birth clouds) and dust. In this Figure the optical depth $\langle \tau_V \rangle$ of both screens are varied. The colour coding corresponds to fixed mean homogeneous optical depths of the screen of dust representing the diffuse dusty ISM. An increase in IRX along a line with fixed colour corresponds to an increase in the homogeneous optical depth of the birth cloud. The red lines show the IRX - β relation for the scenario where the second screen representing the diffuse dust ISM has $\langle \tau_V \rangle = 0$, i.e., stellar emission only passes through the birth cloud. The relations are plotted for different dust types. Homogeneously distributing the birth clouds of stars within a dusty ISM causes variations in the IRX - β relation towards bluer values of β for a fixed IRX.

We show the reconstructed IRX - β relation based on fits to photometric datapoints for different redshifts in Figure 10. The original IRX - β relation based on a direct fit to the attenuated spectra is shown as a black dashed line. The IRX - β relation based on a fit to photometric datapoints can significantly differ from the original IRX - β relation. This is especially evident for MW dust at $z = 0$, $z = 1$, and $z = 8$, driven by contamination of the fit by the 2175 Å bump. At $z = 0$ and $z = 8$ the poor sampling suggests that the attenuated stellar emission is very blue for a given IRX. At $z = 1$ the resulting IRX - β relation is similar to the SMC IRX - β relation (Pettini et al. 1998), even though a MW dust attenuation curve was employed. The same effects are seen for the LMC dust attenuation curve, though less prominently. There is a clear offset between the IRX - β relation based on a fit to photometric datapoints and a fit to the attenuated stellar spectrum for the SMC dust attenuation curve at $z = 1$. This is driven by a poor sampling of the FUV part of the rest-frame spectrum. There is hardly

total IR flux from galaxies based on a limited sampling of the FIR and sub-mm SED or incorrect assumptions on the temperature of the dust (Bouwens et al. 2016; Narayanan et al. 2017). We ignore these effects in this work, but caution the reader to be aware of them.

any difference between the 'observed' and original IRX - β relation for the MW-BUMP00 dust attenuation curve. The MW-BUMP00 attenuation curve doesn't have any strong features and the attenuated stellar spectrum can easily be fit even with only two photometric datapoints.

Additional coverage of the rest-frame NUV wavelength range at $z = 0$ and $z = 8$, as well as additional coverage of the rest-frame FUV wavelength regime at $z = 1$ would improve the reconstruction of the IRX - β relation. We explore other filter combinations in Appendix A and in some cases indeed find a better reconstruction of the IRX - β relation. We list suggested filter combinations as a function of redshift that reliably reconstruct the UV slope β of the IRX - β relation in Table A1.

4 DISCUSSION

In this work we have presented a simple model that puts a screen of dust in front of a young stellar population to study how varying properties of the dust screen and the stellar population cause variations in the IRX - β dust attenuation relation of galaxies. It is worthwhile to separate deviations in two different classes, above and below the original IRX - β relation, or in other words, deviations towards bluer and redder UV colours at fixed IRX. Older stellar populations move

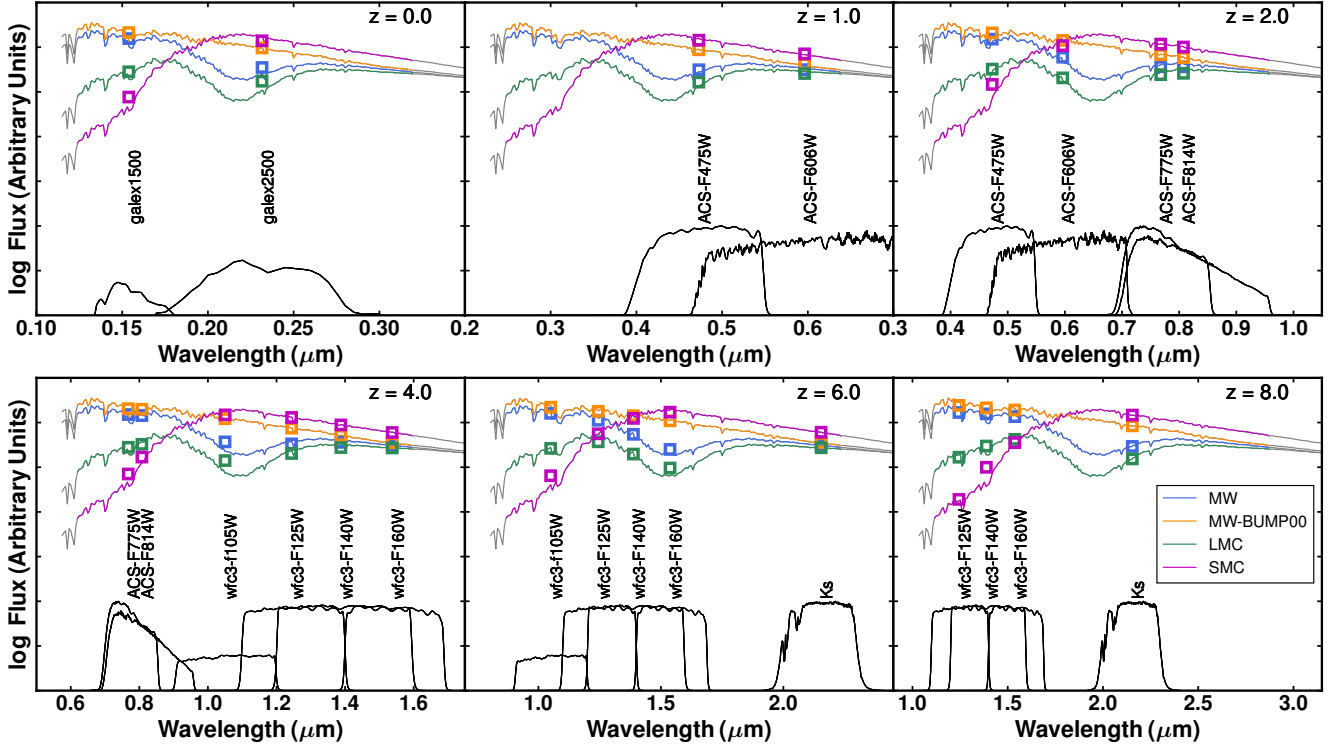


Figure 9. The coverage of the UV rest-frame wavelength regime by different filters for redshifts running from $z = 0$ to $z = 8$, when adopting the four different dust-types in this study. The photometric sampling includes the HST filters that are part of the 3D-HST survey (Skelton et al. 2014), on top of *GALEX*, and a Ks-band filter. The coloured lines mark the attenuated spectra (from rest-frame 1230 to 3200 Å) assuming a V-band optical depth of $\langle \tau_V \rangle = 1$. The relevant filters at each redshift and their transmission curves are plotted below the stellar spectra. The photometric datapoints are marked as coloured squares, where the colours correspond to the attenuated spectra for different dust attenuation curves. The stellar spectra come from a solar-metallicity single-burst population with an age of 10 Myr. The sampling of the filters does not always give a good representation of the original spectrum (e.g., the poor sampling of the absorbed FUV regime at $z = 1$ for the SMC dust type).

the $\text{IRX} - \beta$ relation to redder UV colours. An attenuation curve with a strong FUV component flattens the relation, which results in deviations towards redder UV colours compared to the MW dust attenuation curve. An increased level of turbulence, on the other hand, results in bluer UV slopes at fixed IRX. A small region of unobscured stellar emission (up to a few per cent), the mixing of dust and stars, and a two-component dust model (where dusty birth clouds are located within a diffuse dusty ISM) also results in deviations towards blue UV colours for a given IRX. We schematically depict these effects in Figure 11. In the remaining of this Section we will first focus more on the physics behind the $\text{IRX} - \beta$ relation. We then discuss the origin of variations in the $\text{IRX} - \beta$ relation for different observed classes of galaxies. We finish by discussing the prospects of approximate analytical equations for the $\text{IRX} - \beta$ relation and what future observations can better constrain the $\text{IRX} - \beta$ relation as a function of galaxy type and cosmic epoch.

4.1 The physics behind the $\text{IRX} - \beta$ relation

The $\text{IRX} - \beta$ relation for a uniform screen of dust has a very distinct shape, best described by an asymptotic power law. The individual components (the power law component and the asymptot) have their own physical origin. The asymptot represents a minimum value for the UV slope β and IRX.

The minimum value for β is set by the stellar population itself and corresponds to stellar population age. The minimum value for IRX equals zero, corresponding to a scenario where no emission is absorbed.

The physical origin of the power law can be understood when focusing on the absorption of stellar emission by dust. For a uniform screen of dust the nominator and denominator of $\text{IRX} = L_{\text{IR}}/L_{1600\text{\AA}}$ scale exponentially with the optical depth of the screen, such that

$$L_{\text{IR}} \propto \int_{\lambda, \text{min}}^{\lambda, \text{max}} [1 - \exp(-\tau_{\lambda})] d\lambda$$

and

$$L_{1600\text{\AA}} \propto \exp(-\tau_{1600\text{\AA}}).$$

The UV slope β is set by the slope between FUV and NUV luminosity. Both of these scale exponentially as

$$L_{\lambda, \text{NUV|FUV}} \propto \exp(-\tau_{\lambda, \text{NUV|FUV}}).$$

If we express the optical depths in terms of the V-band optical depth ($\tau_{\lambda} = A(\lambda) \times \tau_V$, where $A(\lambda)$ is a function of wavelength), it immediately becomes clear that both IRX and β exponentially scale with the V-band optical depth τ_V . This makes the exponential dependence on τ_V the driver of the power law trend. In this framework it also becomes clear that as the ratio $A_{\lambda, \text{FUV}}/A_{\lambda, \text{NUV}}$ increases, the slope

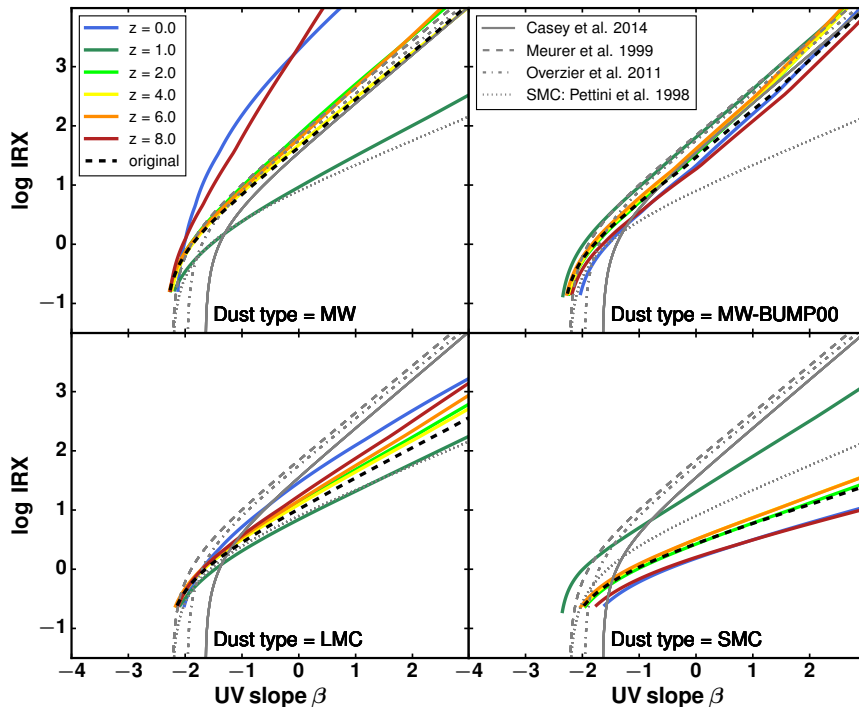


Figure 10. The $IRX - \beta$ relation based on a fit to photometric datapoints for different dust types. The photometric sampling includes the HST filters that are part of the 3D-HST survey (Skelton et al. 2014), on top of *GALEX* filters and a Ks-band filter. Photometric datapoints were obtained by convolving the redshifted stellar spectrum with telescope filters corresponding to the rest-frame wavelength range $1230 < \lambda < 3200 \text{ \AA}$. The black dashed lines correspond to the original $IRX - \beta$ relation derived from a direct fit to the attenuated spectrum. The sampling of telescope filters of the UV wavelength range alters the location of galaxies in the $IRX - \beta$ plane for dust types with a steep UV-slope (SMC dust) or UV absorption features (2175 \AA bump; MW and LMC dust).

of the relation between UV slope β and τ_V steepens. This is the principal cause of the flattening in the $IRX - \beta$ relation for dust attenuation curves with an increased FUV/NUV attenuation ratio (e.g., an SMC curve).

4.2 Observed variations in the $IRX - \beta$ relation

4.2.1 A spatially resolved $IRX - \beta$ relation for local galaxies

Boquien et al. (2012) looked at the $IRX - \beta$ relation on sub-galactic scales in star-forming galaxies as a part of the *Herschel* reference survey (Boselli et al. 2010). The comparison between the Boquien et al. results and our model is interesting, as sub-galactic regions are perhaps more similar to the screen of dust experiment presented in this work than integrated galaxy properties. Boquien et al. (2012) find that for all except one galaxy in their sample, the $IRX - \beta$ relation on sub-galactic scales is located below the Meurer, Heckman & Calzetti (1999) and Overzier et al. (2011) relation for local (blue starburst) galaxies. Our results suggest that stellar age and differences in the dust attenuation curves may cause such variations. Only one galaxy in their sample, NGC 4536 which is undergoing a nuclear starburst, follows the relation for starburst galaxies. An increased level of turbulence or a two-component dust model in starburst environments would naturally cause such a shift, as would a young light-weighted mean stellar age of a few Myr.

Boquien et al. fit SEDs to study variations in the $IRX -$

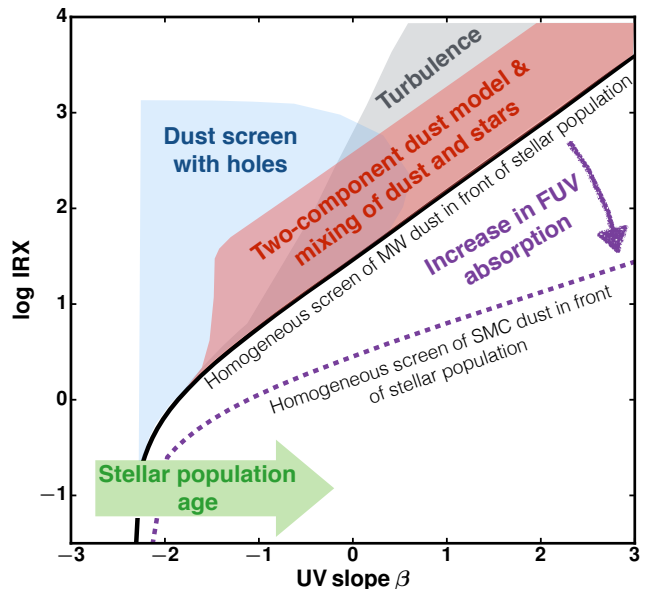


Figure 11. A schematic figure summarising how different physical processes affect the $IRX - \beta$ relation. A patchy screen, turbulence, the mixing of dust and stars, and a two-component dust model yield deviations above the MW $IRX - \beta$ relation, whereas age and an increased FUV absorption component yield deviations below the $IRX - \beta$ relation.

β relation as a function of a number of parameters, including stellar mass, SFR, 4000 Å break index, V-band attenuation, FUV attenuation, mass weighted age, a parameter α tracing dust temperature (Dale & Helou 2002), and the slope of the attenuation curve δ . The authors found that deviations from the Meurer, Heckman & Calzetti (1999) IRX – β relation are poorly described by age sensitive parameters such as the 4000 Å break index, birthrate parameter, and the mass normalised age. Boquien et al. (2012) find that variations can best be described by variations in the intrinsic UV colour in the absence of dust between different sub-galactic regions. Such variations originate from differences in star-formation history (SFH) of the respective regions. Boquien et al. (2012) furthermore conclude that the shape of the attenuation curve can play a secondary role in describing deviations from the Meurer, Heckman & Calzetti (1999) relation. The latter is in agreement with our results of a flattening in the IRX – β relation as the FUV/NUV attenuation ratio increases. The former, intrinsic variations in β due to differences in SFH, is not explored in our model. Such variations should reflect themselves in variations in the light-weighted age (rather than mass normalised age). The light-weighted stellar age can still be a key player that causes the redder UV colours for sub-galactic regions.

Muñoz-Mateos et al. (2009) looked at the IRX – β relation in radial bins of local galaxies from the *Spitzer* Infrared Nearby Galaxies Survey sample (Kennicutt et al. 2003) and found that both β and IRX correlate well with gas-phase metallicity. Observations and theoretical models have demonstrated a clear relation between gas-phase metallicity and dust-to-gas ratio (e.g., Leroy et al. 2011; Rémy-Ruyer et al. 2014; Popping, Somerville & Galametz 2016). An increase in gas-phase metallicity therefore corresponds to an increase in the dust-column and consequently the optical depth seen by the photons. Since both β and IRX scale exponentially with V-band optical depth, this naturally results in a trend between β and IRX and gas-phase metallicity (as long as the gas column the emission travels through doesn't change dramatically from one region to the other). Like Boquien et al. (2012), Muñoz-Mateos et al. (2009) find that starburst galaxies have bluer UV colours than normal star-forming galaxies. As stated before, turbulence driven star formation, a two-component dust model, and young stellar ages naturally cause such blue UV colours.

Ye et al. (2016) looked at the IRX – β relation for individual HII regions in NGC 628. Individual HII regions may be the fairest observational comparison to our model of a screen of dust in front of a single stellar population. Ye et al. (2016) find that H α equivalent width (an age tracer) significantly correlates with deviations from the local (blue starburst) IRX – β relation. As the equivalent width decreases (older stellar populations) the HII regions have redder UV colours β . Ye et al. furthermore find that stellar population age and the 4000 Å break also moderately correlate with deviations. This is in good agreement with our conclusion that older stellar populations drive variations towards red UV colours (see also, Kong et al. 2004; Grasha et al. 2013, and many others). Ye et al. (2016) also find that metallicity and Balmer decrement show no correlation with deviations from the IRX – β relation.

4.2.2 SMC dust in early galaxies

Capak et al. (2015), Bouwens et al. (2016), Pope et al. (2017), and Smit et al. (2017) observed a number of high-redshift ($z > 4$) galaxies with a UV-slope $\beta \sim -1$ and IRX ~ 1 or less. These works concluded that these values are consistent with an SMC attenuation curve, suggesting that dust in early Universe galaxies is similar to SMC dust. We found that deviations towards red UV-slopes with respect to the canonical IRX – β relations are driven by either an ageing stellar population or by varying dust types. Similar values for β and IRX as observed by Capak et al. (2015), Bouwens et al. (2016), Pope et al. (2017), and Smit et al. (2017), can be obtained when the stellar emission from a 50–100 Myr old stellar population passes through a screen of dust with a MW attenuation curve. The effect of ageing has been discussed before by many authors (e.g., Kong et al. 2004; Grasha et al. 2013).

Without additional information on the age of the observed stellar population it is hard to disentangle dust attenuation curve versus age. Some additional insight can still be gained when taking the typical lifetime of molecular clouds into account. Assuming that stars leave their birth clouds after 5–20 Myr (the lifetime of molecular clouds, Murray, Quataert & Thompson 2010), strong deviations towards red UV-slopes of $\beta = -1$ for low values of IRX are more likely to be driven by changes in the dust attenuation curves (the stellar populations are too young to cause significant shifts in the IRX – β relation). Furthermore, older stellar populations should not be a large concern at higher redshifts given the much smaller stellar population ages and much higher specific star formation rates in galaxies at high redshifts. The bright UV and IR emission (and in some cases [CII] emission) detected in early Universe galaxies indeed suggest that these galaxies are actively star forming and likely have a UV spectrum dominated by young stars. This favours an SMC attenuation curve over a MW curve for the $z > 4$ galaxies.

Narayanan et al. (2017) suggested that the low IRX values observed in $z > 4$ galaxies are due to a poor assumption for the dust temperature, rather than SMC dust attenuation curves (see also Ferrara et al. 2016). When only a handful of photometric datapoints are available for the IR wavelength regime, the total infrared luminosity is estimated based on an assumption for the dust temperature. Narayanan et al. (2017) compared the dust temperatures of galaxies in hydrodynamical models to assumed dust temperatures and found that the assumed temperatures for high-redshift galaxies are often lower than the dust temperatures suggested by the models. An increase in the assumed dust temperature naturally increases the total infrared luminosity and IRX towards a MW IRX – β relation. Bouwens et al. (2016) also concludes that the dust temperature of galaxies might increase with look-back time, based on the large number of non-detected galaxies at 3mm continuum in ASPECS (The ALMA Spectroscopic Survey in the Hubble Ultra Deep Field, Walter et al. 2016). A better photometric sampling of the Rayleigh-Jeans tail of the sub-mm SED of high-redshift galaxies is necessary and will provide valuable insights.

Recently, Reddy et al. (2017, see also Reddy et al. (2012)) found that normal star-forming galaxies at $1.5 \leq z \leq 2.5$ have values for IRX and β that correspond best

to an SMC dust attenuation curve. Siana et al. (2008) and Siana et al. (2009) found similar results for lensed Lyman Break galaxies at $z \sim 3$. The hypothesis of a dust temperature that is too low can not be valid for the SMC attenuation curves favoured in these works. Good *Spitzer* and *Herschel* coverage of the peak of the IR SEDs is available for these galaxies. A lack of information about the SED at millimetre wavelengths can still introduce a bias towards low IRX values. The *Herschel* photometry is sensitive to the warm dust, and may miss the contribution to the total IR luminosity from a large cold dust component (although more than half of the IR flux has to come from the cold component for IRX to align with a MW dust curve).

There appears to be some tension between the Siana et al. and Reddy et al. results and the result of studies of the IRX – β relation for bright UV-selected galaxies at the same redshifts that found an IRX – β relation similar to the local (blue starburst) relation (e.g., Heinis et al. 2013; Coppin et al. 2015; Álvarez-Márquez et al. 2016). Differences in SFH may play a role here (for instance young stars driving the bright UV emission in UV-selected galaxies), but there is evidence that differences in the attenuation curves may really be the key driver of the SMC IRX – β relation. Kriek & Conroy fit composite SEDs with flexible stellar population synthesis models to galaxies, while exploring attenuation curves with varying slopes and UV bump strengths (see also Salmon et al. 2016). They find that star-forming galaxies at $z \sim 2$ on average have an attenuation curve with a slope between MW and SMC and a weak presence of a 2175 Å bump (25% of the MW bump). They furthermore find that galaxies with larger specific SFRs have shallower extinction curves. Unfortunately our model is not equipped to relate different dust types to galaxy properties such as stellar mass and SFR.

If any conclusion has to be reached based on the apparent SMC IRX – β relation in $z > 4$ galaxies and star-forming galaxies at $z \sim 2$, it is that good coverage of the entire SED of galaxies from the UV to the sub-mm is necessary to properly assess the IRX – β relation in different types of galaxies. The good coverage allows for a careful determination of both β and IRX, while simultaneously providing constraints on the dust attenuation curve.

If dust attenuation curves vary between SMC and MW type from one galaxy to the other, this is an interesting result in itself. The SMC dust model is generally thought to better represent the dust properties of galaxies in the early Universe than a MW dust model. This is motivated by the low metallicities these galaxies are thought to have and a dust population dominated by dust produced in SNe and through the accretion of metals onto dust grains (e.g., Zhukovska & Henning 2013; Popping, Somerville & Galametz 2016). Massive main-sequence galaxies at $z \sim 2$ on the other hand have metallicities close to solar (e.g., Zahid et al. 2013) and therefore this argument doesn't hold for these objects. Furthermore, at these redshifts dust produced in active giant branch stars becomes increasingly more important, likely changing the dust attenuation curve. Shattering of grains promotes the production of small grains and strong FUV attenuation (Hirashita 2010). This may play a key role in the turbulent ISM of massive and actively star-forming galaxies at $z \sim 2$ and thus be the real driver of SMC attenuation curves and SMC IRX – β relations. At the

same time shattering can be balanced by the coagulation of grains in dense media (Hirashita & Voshchinnikov 2014; Hirashita 2015) and result in MW type attenuation curves. Besides observational efforts, it is thus of key importance that cosmological galaxy formation models address the origin of dust attenuation curves in different galaxy types over cosmic time, accounting for the many processes that shape attenuation curves (e.g., different dust formation mechanisms and grain-grain collisions).

4.2.3 Geometry effects make galaxies blue

Observations of high-redshift dusty star-forming galaxies have suggested that galaxies become bluer as their infrared luminosity increases (e.g., Penner et al. 2012; Oteo et al. 2013; Casey et al. 2014; Bourne et al. 2017). In our model there are multiple competing effects that can cause the UV-slope β to shift to lower values at fixed IRX (turbulence, a small fraction of stellar emission not covered by dust, a uniform mixing of stars within the dust screen, two-component dust model). For example, a two-component dust model can describe the location in the IRX – β plane of a large fraction of the blue low- and high-redshift DSFGs. Given that DSFGs are very dust-rich systems, the effects of the two-component dust model and the IRX – β relation are very likely to play an important role (a large optical depth of the ‘diffuse’ dusty ISM).

Although with varying degree, all these aforementioned effects result in some fraction of the stellar emission being completely absorbed and driving IRX, whereas the remaining fraction of the original stellar emission is hardly absorbed and responsible for the observed UV emission. For young stellar populations, this results in blue UV-slopes β . In summary, blue galaxies with a strong IR component are the result of spatial variations in the optical depth through which the stellar emission travels (see also e.g., Casey et al. 2014). Koprowski et al. (2016) and Chen et al. (2015) have shown significant offsets between the origin of the rest-UV/optical and sub-mm emission in DSFGs. Similarly, Puglisi et al. (2017) showed that in $z \sim 1.6$ off-main-sequence galaxies the Balmer decrement (i.e. an optical dust attenuation tracer) yields a dust attenuation much lower than the attenuation one would derive from the observed IRX. These results demonstrate that UV/optical and IR emission can originate from very different regions and therefore can not be approximated by a single uniform screen of dust. Similar conclusions were reached by other theoretical efforts to understand the nature of blue DSFGs (Safarzadeh, Hayward & Ferguson 2017; Narayanan et al. 2017), although these works did not explore all the geometry effects presented in this work.

It is worthwhile to focus a bit more on the effect of turbulence on the IRX – β relation. An increased level of turbulence may be important for dust absorption in stellar birth clouds. Giant Molecular Clouds (GMCs) in our Milky Way and in local galaxies have significant non-thermal line widths (e.g., Fukui et al. 2001; Elmegreen & Scalo 2004), a signature of the presence of supersonic turbulence. Swinbank et al. (2011) found a highly turbulent ISM in a dusty star-forming galaxy at $z = 2$. Supersonic turbulence in the birth clouds of young stars can thus naturally cause deviations away from the canonical IRX – β relation and can

Table 1. Best fit parameters for the analytic approximation of the IRX – β relation invoking dust type, stellar population age, and turbulence of the dust screen (Equations 3 to 6).

Dust type	A_{screen}	B_{screen}	C_{screen}	A_{turb}	B_{turb}	C_{turb}	D_{turb}	E_{turb}	$A_{\delta\beta}$	$B_{\delta\beta}$	$C_{\delta\beta}$
MW	0.69	4.17	1.72	0.05	5.89	2.8	0.41	0.37	0.05	0.74	1.11
MW-BUMP00	0.45	4.65	1.89	0.03	5.44	2.52	0.44	0.41	0.08	0.72	1.14
LMC	0.78	2.66	1.09	0.06	3.53	1.76	0.42	0.35	0.17	0.7	1.24
SMC	0.66	1.84	0.75	2.01	-0.06	0.64	-2.24	0.66	0.39	0.63	1.54

be responsible for at least a fraction of the scatter around the observed IRX – β relations. Casey et al. (2014) found that local galaxies with SFRs larger than $25 M_{\odot} \text{ yr}^{-1}$ are typically located above their observed best-fit IRX – β relation for local galaxies (i.e., bluer than expected) and that the deviation from the canonical IRX – β relations for high redshift DSFGs increases as a function of FIR luminosity. Empirical fits of the IRX – β relation for local starbursts (Meurer, Heckman & Calzetti 1999; Overzier et al. 2011) suggest bluer UV colours than fits to local ‘normal’ star-forming galaxies (Casey et al. 2014, see also Boquien et al. (2012)). An increased level of turbulence in the birth clouds or the diffuse ISM of starbursts is one of the possible explanations for this.

Unfortunately, without detailed measurements of the turbulence within molecular clouds and the diffuse ISM it is hard to quantify how much of the deviations away from the IRX – β relation can be accounted for by a turbulent dust screen. Absorption studies probing non-thermal line widths towards turbulent regions in the Milky Way or local galaxies could potentially shed more light on this. The high-spatial resolution capabilities of the Atacama Large (sub-)Millimeter Array (ALMA) can resolve GMCs in nearby galaxies. This makes ALMA an ideal instrument for such an exercise. An interesting alternative would be to study deviations from the IRX – β relation in galaxies as a function of star-formation efficiency. The turbulence within molecular clouds is intimately related to the efficiency with which stars form (Krumholz & McKee 2005). One could thus expect galaxies to become bluer as the star-formation efficiency increases (or the molecular hydrogen depletion time decreases). It is furthermore worthwhile to study deviations from the IRX – β relation as a function of galaxy velocity dispersion.

We want to spend a few more words focusing on the two-component dust model, in which dusty birth clouds are homogeneously distributed within a diffuse dusty ISM. First of all, the effects of this model only become important once the optical depth $\langle \tau_{\nu} \rangle$ of the diffuse dusty ISM is larger than approximately four. As stated before, this limits the importance of this model to very dust-rich systems (e.g., DSFGs). Locally, reddening of light in birth clouds is approximately 2 times stronger than reddening of light in the diffuse ISM (Calzetti et al. 2000). Puglisi et al. (2016) showed that for far-IR selected normal star-forming galaxies at $z \sim 1$ the reddening of light in birth clouds is roughly similar to the reddening of light in the diffuse ISM. This suggests that birth clouds have a larger filling factor in galaxies at $z \sim 1$ than locally.

4.3 Analytic approximation for the IRX – β relation

One of the main motivations for the IRX – β relation is that it can potentially account for absorbed UV emission. Variations in the IRX – β relation unfortunately complicate this. Only if these deviations can be described as a function of other parameters can the IRX – β relation really be used to account for obscured SF.

Safarzadeh, Hayward & Ferguson (2017) conclude that variations in the dust composition are the dominant source of variations in the IRX – β relation in their simulations. Kong et al. (2004) suggested that the ratio of the present to past average SFR defines the deviation of galaxies away from the canonical Meurer et al. IRX – β relation. This was contradicted by Johnson et al. (2007), Boquien et al. (2012), and Johnson et al. (2013) who find that the dispersion in UV-slope β hardly correlates with the star-formation history of galaxies as traced through their 4000 Å break. Grasha et al. (2013) found that deviations away from the IRX – β relation can be described by the mean stellar age of the galaxies (but see Boquien et al. 2012). We also find that the stellar population age drives the UV-slope β towards higher values.

Narayanan et al. (2017) concludes that besides age, the total SFR (or IR luminosity) of a galaxy is an important parameter that controls the deviation of galaxies away from the canonical IRX – β relation. This would be in line with the $z = 0$ sample presented in Casey et al. (2014), who found that galaxies lie increasingly above the best-fit IRX – β relation as a function of SFR and IR luminosity. As discussed in Section 4.2.3, the underlying physical motivation for this might be an increase in the turbulence within the birth clouds of young stars.

Our results show that the origin of deviations away from local fits of the IRX – β relation is much more complicated and can not simply be captured by a combination of stellar age and SFR (turbulence). Besides these two parameters, the attenuation curve of the screen of dust, the mixing of stars within the screen of dust, a two-component dust model, and the covering fraction of the dust all contribute heavily to deviations away from the IRX – β relation. As an experiment we could imagine a galaxy for which a UV-slope β of -1 is observed and a mean stellar age of 10 Myr is determined. If only turbulence would play a role, the range in IRX one could get covers approximately 0.2 dex for a MW dust attenuation curve. The assumption of a two-component dust model or that stars and dust are mixed increases the range in acceptable IRX values to about ~ 0.6 dex. If no information is available for the dust attenuation curve of the galaxy, the range in possible IRX values increases to ~ 1.5

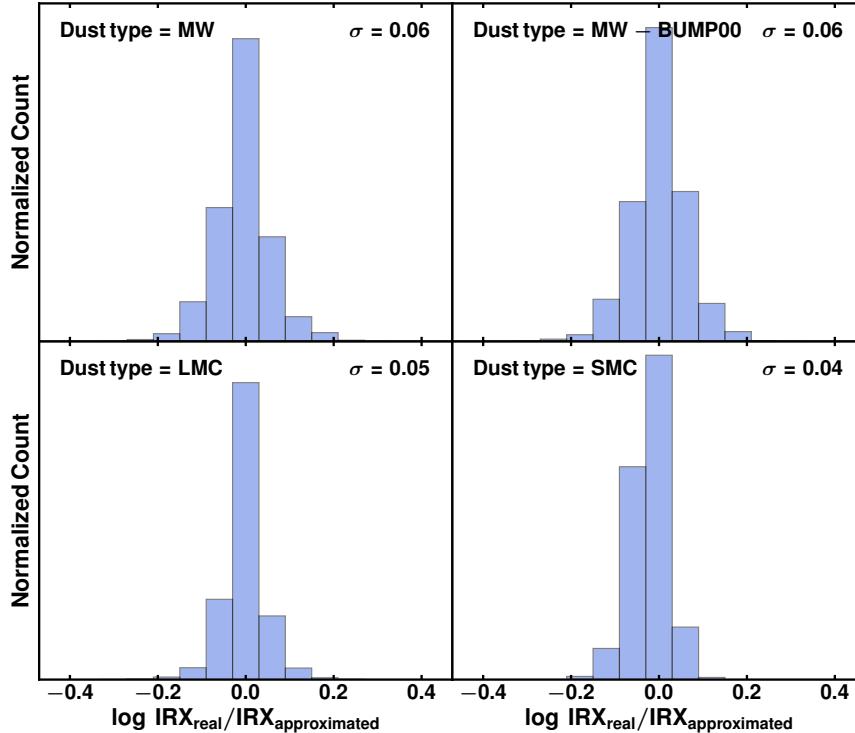


Figure 12. The distribution of the log of the uncertainty (i.e. $\log[\text{IRX}_{\text{real}}/\text{IRX}_{\text{approximated}}]$) in IRX based on the analytic approximation for the IRX – β relation (Equations 3 to 6) for the four different dust types discussed in this work. This plot was created by running 25 000 combinations of homogeneous V-band optical depth ($\langle \tau_V \rangle$ running from 1 to 20), Mach number (running from $\mathcal{M} = 0$ to $\mathcal{M} = 4$), and stellar population age (from 5 to 100 Myr) for each dust type (see Sec. 4.3 for a detailed description).

dex. Without prior information on the covering fraction of the dust the range of possible IRX values increases up to three orders of magnitude. Such variations are not covered anymore by two parameters, but require detailed spatially resolved information about the galaxy and full SED fitting to constrain the most likely dust attenuation curve (e.g., Noll et al. 2009; Kriek & Conroy 2013; Salmon et al. 2016).

An additional complication to the parametrisation of deviations are observational effects. As demonstrated in Section 3.5, the sampling of the stellar SED by telescope filters can lead to systematic variations in the location of galaxies within the IRX – β plane. Lastly, ideally deviations away from the IRX – β relation can be parametrised as a function of properties that can be determined from the UV spectrum alone, unlike age and total SFR.

Despite the negative tone, it is still worthwhile to find an approximate analytic equation for the IRX – β relation that includes a subset of the discussed physical processes. Here we focus on an approximation that includes the effects of stellar population age and turbulence for the four different attenuation curves discussed in this work. These approximations can be useful in case good arguments can be made that a screen of dust without holes is a good approximation of the dust distribution in a galaxy (e.g., if the non-obscured UV emission escaping through these holes is too faint to observe). Accounting for stellar age and turbulence we can fit the relation between IRX and β using the following set of

equations:

$$\text{IRX}(\beta, \text{Age}, \mathcal{M}) = \text{IRX}_{\text{screen}}(\beta, \text{Age}) + \text{IRX}_{\text{turb}}(\beta, \text{Age}, \mathcal{M}) \quad (3)$$

where

$$\text{IRX}_{\text{screen}}(\beta, \text{Age}) = A_{\text{screen}} \times \left[10^{0.4[B_{\text{screen}} + C_{\text{screen}}(\beta - \delta\beta)]} - 1 \right], \quad (4)$$

$$\text{IRX}_{\text{turb}}(\beta, \text{Age}, \mathcal{M}) = A_{\text{turb}} \times \left[10^{0.4[B_{\text{turb}}\mathcal{M}^{D_{\text{turb}}} + C_{\text{turb}}\mathcal{M}^{E_{\text{turb}}}(\beta - \delta\beta)]} - 1 \right], \quad (5)$$

and

$$\delta\beta(\text{Age}) = \exp[A_{\delta\beta} + B_{\delta\beta} \times \log(\text{Age}/10 \text{ Myr})] - C_{\delta\beta}. \quad (6)$$

We set IRX_{turb} to zero when $\text{IRX}_{\text{turb}} < 0$ (as this marks an unphysical scenario with negative IR luminosities). $\text{IRX}_{\text{screen}}$ marks the IRX one would get for a uniform screen of dust. IRX_{turb} is a correction that accounts for the turbulence within the screen. When $\mathcal{M} = 0$, a uniform screen, IRX_{turb} will automatically equal zero. $\delta\beta(\text{Age})$ takes the shift in β due to stellar population age into account. The best-fit parameters for Equations 3 to 6 are listed in Table 1.

We tested our analytic approximation for 25 000 different combinations of homogeneous V-band optical depth (running from 1 to 20), Mach number (running from $\mathcal{M} = 0$

to $\mathcal{M} = 4$), and stellar population age (from 5 to 100 Myr). We first calculated the real IRX and β for each of these combinations using the approach outlined in Section 2. This resulted in IRX_{real} and β_{real} . We then used the analytic approximation presented in Equations 3 to 6 to calculate $\text{IRX}_{\text{approximated}}$ as a function of β_{real} , as well as the stellar population age and Mach number that went into the calculation for IRX_{real} .

We quantify the uncertainty in $\text{IRX}_{\text{approximated}}$ in Figure 12 by showing the difference between the real and approximated IRX ($\log[\text{IRX}_{\text{real}}/\text{IRX}_{\text{approximated}}]$) for a given $\langle \tau_V \rangle$, stellar population age, and Mach number (and β_{real}). The typical one-sigma uncertainty in $\text{IRX}_{\text{approximated}}$ is ~ 0.05 dex, which suggests that our analytic expression is a good representation of the IRX – β relation. If turbulence is indeed correlated with SFR, non-thermal line width, SFE, or velocity dispersion, similar empirical equations could be derived as a function of these galaxy properties. We remind the reader that the presented analytic equation does not include the effects of a patchy dust screen or the mixing of dust and stars.

4.4 Future prospects to use the IRX – β relation to estimate the intrinsic SFR of galaxies

Although the large theoretical scatter in the IRX – β relation seems to be discouraging for its use as a tracer of absorbed UV emission, this does not necessarily need to be. If the IRX – β relation for galaxies of certain types at certain epochs can be constrained, these constrained relations may still be valuable when estimating the obscured UV emission of galaxies. For instance, the IR-brightest $z \sim 2$ DSFGs appear to suffer more from dust geometry effects than normal star-forming galaxies at these redshifts (e.g., Penner et al. 2012; Oteo et al. 2013; Casey et al. 2014). High spatial resolution observations and/or good SED coverage of the rest-frame UV wavelength over large redshift ranges make detailed studies of the IRX – β relation for individual galaxy populations over cosmic time possible.

NIRCam on board of the *James Webb Space Telescope* (JWST) will offer up to 0.1 arcsec imaging of the entire UV rest-frame wavelength regime of galaxies at $z \geq 3$. Combined with the exquisite spatial resolution of ALMA to probe the sub-mm emission of galaxies, this opens up the possibility of a detailed resolved study of large scale dust geometry effects in galaxies (differences in location of the UV and IR emission). The good photometric sampling of the rest-frame UV of galaxies at $z \geq 3$ by NIRCam enables SED fitting of the rest-frame UV spectrum. This provides essential insights into the properties of the dust (e.g., the presence of a 2175 Å bump and the slope of the attenuation curve). Large scale geometry effects and differences in the dust attenuation curve are among the physical processes that cause largest variations in the IRX – β relation. The combination of JWST and ALMA to obtain spatially resolved imaging is thus a perfect approach to constrain the IRX – β relation for different types of galaxies over a large redshift range (including normal star-forming galaxies, DSFGs, and galaxies during the epoch of reionization), where different physical processes may dominate.

Other instruments such as the Euclid and the Wide-Field Infrared Survey Telescope (WFIRST) will provide

good sampling of the rest-frame UV of high-redshift galaxies on large areas on the sky (though at a lower spatial resolution than JWST and depending on the redshift the rest-frame UV spectrum is not entirely covered). Unfortunately, ALMA is not in the position to follow up all the sources that will be detected by these future NIR space observatories (including JWST). Nevertheless, constraints on the dust attenuation curves in different classes of galaxies through the SED fitting of the photometric sampling of the rest-frame UV on itself is valuable to better constrain the IRX – β relation of galaxies (and in general the dust properties).

Although challenging, future small sample studies to constrain the IRX – β relation and/or some of the physical processes that cause variations for different galaxy types at different epochs will justify the use of the IRX – β relation to reliably estimate the obscured UV emission and intrinsic SFR of galaxies.

5 SUMMARY & CONCLUSIONS

The IRX – β relation is commonly used to estimate the intrinsic SFR in galaxies when no IR/sub-mm information is available. In this paper we have presented a simple model to explore how different physical effects cause variations in the IRX – β dust attenuation relation. We place a screen of dust in between a young stellar population and the observer and vary the properties of the dust screen and the age of the stars. The attenuation of stellar light is modelled by applying attenuation curves presented in Seon & Draine (2016), who perform radiative transfer calculations in a spherical, clumpy interstellar medium. We summarise our main findings below:

- Our simple model can reproduce the observed IRX – β relation for local (blue starburst) galaxies as presented in Meurer, Heckman & Calzetti (1999), Overzier et al. (2011), and Casey et al. (2014) when invoking a uniform screen of MW type dust in front of a stellar population with an age of ~ 10 Myr. The asymptotic power law relation between IRX and β as found in the literature and suggested by our models is driven by the exponential dependence of both β and IRX on the V-band optical depth.

- An increase in stellar population age increases the UV slope β , and moves galaxies to higher values of β for a fixed IRX.

- An increase in the FUV absorption with respect to longer wavelengths flattens the IRX – β dust attenuation relation, driven by a steeper UV slope β . This effect is apparent when comparing the IRX – β relation for MW, LMC, and SMC dust types.

- An increased level of turbulence in the screen of dust leads to lower values for both β and IRX, in such a way that galaxies move towards locations in the IRX – β plane above the relation for a uniform dust screen. For a fixed IRX, galaxies become bluer.

- A patchy distribution of dust with holes in it causes strong deviations from the IRX – β relation for a uniform dust screen, with blue UV colours combined with high values for IRX.

- When stars are mixed in between the screen of dust rather than placed in front of it, both β and IRX decrease, causing deviations towards bluer UV colours for a given IRX.

- A two-component dust model, where dusty birth clouds are distributed within the diffuse ISM, also causes deviations towards blue UV colours for a given IRX.

- A poor photometric sampling of the rest-frame UV spectrum can artificially move galaxies around the IRX – β plane. A remedy for this is a filter combination that at least probes the rest-frame FUV (~ 1250 Å) and rest-frame NUV (~ 3000 Å) wavelengths.

Taken together, dust geometry effects cause variations towards blue UV colours, whereas strong FUV absorption and stellar age cause variations towards red UV colours for a fixed IRX.

Our results demonstrate that there are numerous competing processes that may simultaneously take place that can move galaxies around the IRX – β plane. More simply put, there exists no universal IRX – β dust attenuation relation. We present an analytical approximation for the IRX – β relation when there are good reasons to believe that all the stellar emission is (up to some extent) absorbed by dust. High-resolution imaging studies of the IRX – β relation combining for instance NIRCам on board of JWST with ALMA will constraint the IRX – β relation for different galaxy types at different epochs where different physical processes that cause variations dominate. These studies are challenging, but in turn will open up the reliable use of the IRX – β relation to estimate the intrinsic SFR of galaxies, despite the lack of a universal IRX – β dust attenuation relation.

ACKNOWLEDGEMENTS

We thank the anonymous referee for useful comments that helped clarify this paper. We thank Chian-Chou Chen, Richard Ellis, Katharina Immer, Desika Narayanan, Ralf Siebenmorgen, Wuji Wang, and Anita Zanella for valuable conversations. We thank Desika Narayanan and especially Richard Ellis for commenting on an earlier version of this paper. GP thanks Claus Leitherer for his support in running *Starburst99*. CN thanks ESO for its hospitality during a long-term visit.

References

- Álvarez-Márquez J. et al., 2016, *A&A*, 587, A122
 Bell E. F., 2002, *ApJ*, 577, 150
 Bell E. F., Gordon K. D., Kennicutt, Jr. R. C., Zaritsky D., 2002, *ApJ*, 565, 994
 Boquien M. et al., 2012, *A&A*, 539, A145
 —, 2009, *ApJ*, 706, 553
 Boselli A. et al., 2010, *PASP*, 122, 261
 Bourne N. et al., 2017, *MNRAS*, 467, 1360
 Bouwens R. J. et al., 2016, *ApJ*, 833, 72
 —, 2011, *ApJ*, 737, 90
 —, 2015, *ApJ*, 803, 34
 Buat V. et al., 2005, *ApJ*, 619, L51
 Burgarella D., Buat V., Iglesias-Páramo J., 2005, *MNRAS*, 360, 1413
 Calzetti D., 1997, *AJ*, 113, 162
 Calzetti D., Armus L., Bohlin R. C., Kinney A. L., Koornneef J., Storchi-Bergmann T., 2000, *ApJ*, 533, 682
 Capak P. L. et al., 2015, *Nature*, 522, 455
 Casey C. M. et al., 2014, *ApJ*, 796, 95
 Charlot S., Fall S. M., 2000, *ApJ*, 539, 718
 Chen C.-C. et al., 2015, *ApJ*, 799, 194
 Coppin K. E. K. et al., 2015, *MNRAS*, 446, 1293
 Cortese L. et al., 2006, *ApJ*, 637, 242
 Cortese L., Boselli A., Franzetti P., Decarli R., Gavazzi G., Boissier S., Buat V., 2008, *MNRAS*, 386, 1157
 Cullen F., McLure R. J., Khochfar S., Dunlop J. S., Dalla Vecchia C., 2017, *MNRAS*, 470, 3006
 Dale D. A., Helou G., 2002, *ApJ*, 576, 159
 Dunlop J. S., McLure R. J., Robertson B. E., Ellis R. S., Stark D. P., Cirasuolo M., de Ravel L., 2012, *MNRAS*, 420, 901
 Ekström S. et al., 2012, *A&A*, 537, A146
 Ellis R. S. et al., 2013, *ApJ*, 763, L7
 Elmegreen B. G., Scalo J., 2004, *ARA&A*, 42, 211
 Ferrara A., Hirashita H., Ouchi M., Fujimoto S., 2016, *ArXiv e-prints* 1607.01824
 Fischera J., Dopita M., 2005, *ApJ*, 619, 340
 Fischera J., Dopita M. A., Sutherland R. S., 2003, *ApJ*, 599, L21
 Fudamoto Y. et al., 2017, *ArXiv e-prints* 1705.01559
 Fukui Y., Mizuno N., Yamaguchi R., Mizuno A., Onishi T., 2001, *PASJ*, 53, L41
 Georgy C. et al., 2013, *A&A*, 558, A103
 Gil de Paz A. et al., 2007, *ApJS*, 173, 185
 Goldader J. D., Meurer G., Heckman T. M., Seibert M., Sanders D. B., Calzetti D., Steidel C. C., 2002, *ApJ*, 568, 651
 Granato G. L., Lacey C. G., Silva L., Bressan A., Baugh C. M., Cole S., Frenk C. S., 2000, *ApJ*, 542, 710
 Grasha K., Calzetti D., Andrews J. E., Lee J. C., Dale D. A., 2013, *ApJ*, 773, 174
 Heinis S. et al., 2013, *MNRAS*, 429, 1113
 Hirashita H., 2010, *MNRAS*, 407, L49
 —, 2015, *MNRAS*, 447, 2937
 Hirashita H., Voshchinnikov N. V., 2014, *MNRAS*, 437, 1636
 Johnson B. D. et al., 2007, *ApJS*, 173, 392
 —, 2013, *ApJ*, 772, 8
 Kennicutt R. C., Evans N. J., 2012, *ARA&A*, 50, 531
 Kennicutt, Jr. R. C. et al., 2003, *PASP*, 115, 928
 Kong X., Charlot S., Brinchmann J., Fall S. M., 2004, *MNRAS*, 349, 769
 Koprowski M. P. et al., 2016, *ApJ*, 828, L21
 Kriek M., Conroy C., 2013, *ApJ*, 775, L16
 Kroupa P., 2002, *Science*, 295, 82
 Krumholz M. R., McKee C. F., 2005, *ApJ*, 630, 250
 Laporte N. et al., 2017, *ApJ*, 837, L21
 Leitherer C. et al., 1999, *ApJS*, 123, 3
 Leroy A. K. et al., 2011, *ApJ*, 737, 12
 Mancini M., Schneider R., Graziani L., Valiante R., Dayal P., Maio U., Ciardi B., 2016, *MNRAS*, 462, 3130
 McLeod D. J., McLure R. J., Dunlop J. S., Robertson B. E., Ellis R. S., Targett T. A., 2015, *MNRAS*, 450, 3032
 Meurer G. R., Heckman T. M., Calzetti D., 1999, *ApJ*, 521, 64
 Muñoz-Mateos J. C. et al., 2009, *ApJ*, 701, 1965
 Murray N., Quataert E., Thompson T. A., 2010, *ApJ*, 709, 191

Narayanan D., Dave R., Johnson B., Thompson R., Conroy C., Geach J. E., 2017, ArXiv e-prints 1705.05858

Noll S., Burgarella D., Giovannoli E., Buat V., Marcillac D., Muñoz-Mateos J. C., 2009, *A&A*, 507, 1793

Oesch P. A., Bouwens R. J., Illingworth G. D., Franx M., Ammons S. M., van Dokkum P. G., Trenti M., Labbé I., 2015, *ApJ*, 808, 104

Oesch P. A. et al., 2014, *ApJ*, 786, 108

Oteo I. et al., 2013, *A&A*, 554, L3

Overzier R. A. et al., 2011, *ApJ*, 726, L7

Pannella M. et al., 2009, *ApJ*, 698, L116

Panuzzo P., Granato G. L., Buat V., Inoue A. K., Silva L., Iglesias-Páramo J., Bressan A., 2007, *MNRAS*, 375, 640

Penner K. et al., 2012, *ApJ*, 759, 28

Pettini M., Kellogg M., Steidel C. C., Dickinson M., Adelberger K. L., Giavalisco M., 1998, *ApJ*, 508, 539

Pope A. et al., 2017, *ApJ*, 838, 137

Popping G., Somerville R. S., Galametz M., 2016, ArXiv e-prints 1609.08622

Puglisi A. et al., 2017, *ApJ*, 838, L18

—, 2016, *A&A*, 586, A83

Reddy N. et al., 2012, *ApJ*, 744, 154

Reddy N. A., Erb D. K., Pettini M., Steidel C. C., Shapley A. E., 2010, *ApJ*, 712, 1070

Reddy N. A. et al., 2017, ArXiv e-prints 1705.09302

Reddy N. A., Steidel C. C., Pettini M., Adelberger K. L., Shapley A. E., Erb D. K., Dickinson M., 2008, *ApJS*, 175, 48

Rémy-Ruyer A. et al., 2014, *A&A*, 563, A31

Safarzadeh M., Hayward C. C., Ferguson H. C., 2017, *ApJ*, 840, 15

Salmon B. et al., 2016, *ApJ*, 827, 20

Seibert M. et al., 2005, *ApJ*, 619, L55

Seon K.-I., Draine B. T., 2016, *ApJ*, 833, 201

Siana B. et al., 2009, *ApJ*, 698, 1273

Siana B., Teplitz H. I., Chary R.-R., Colbert J., Frayer D. T., 2008, *ApJ*, 689, 59

Skelton R. E. et al., 2014, *ApJS*, 214, 24

Smit R. et al., 2017, ArXiv e-prints 1706.04614

Smit R., Bouwens R. J., Labbé I., Franx M., Wilkins S. M., Oesch P. A., 2016, *ApJ*, 833, 254

Strandet M. L. et al., 2017, ArXiv e-prints 1705.07912

Swinbank A. M. et al., 2011, *ApJ*, 742, 11

Takeuchi T. T., Yuan F.-T., Ikeyama A., Murata K. L., Inoue A. K., 2012, *ApJ*, 755, 144

To C.-H., Wang W.-H., Owen F. N., 2014, *ApJ*, 792, 139

Walter F. et al., 2016, *ApJ*, 833, 67

Watson D., Christensen L., Knudsen K. K., Richard J., Gallazzi A., Michałowski M. J., 2015, *Nature*, 519, 327

Weingartner J. C., Draine B. T., 2001, *ApJ*, 548, 296

Wijesinghe D. B. et al., 2011, *MNRAS*, 415, 1002

Ye C., Zou H., Lin L., Lian J., Hu N., Kong X., 2016, *ApJ*, 826, 209

Zahid H. J., Geller M. J., Kewley L. J., Hwang H. S., Fabricant D. G., Kurtz M. J., 2013, *ApJ*, 771, L19

Zhukovska S., Henning T., 2013, *A&A*, 555, A99

APPENDIX A: DEVIATIONS FROM THE IRX – β RELATION DUE TO OBSERVATIONAL EFFECTS: ADDITIONAL FILTER COMBINATIONS

We explored the effect of poor photometric sampling of the rest-frame UV spectra on the derived IRX – β relation in Section 3.5. The exact choice of filters affects the quality of the sampling of the rest-frame UV spectrum. Here we present the sampling of the rest-frame UV spectrum and the resulting IRX – β relation using different combinations of filters.

Figure A1 shows the coverage of the UV rest-frame wavelength regime using *GALEX* and a Ks-band filter, as well as the filters that are part of the 3D-HST survey (Skelton et al. 2014) and two additional HST UVIS filters (UVIS-F275W and UVIS-F336W, as in Reddy et al. 2017). The addition of the UVIS filters compared to the filter set used in Figure 9 improves the sampling of the rest-frame NUV spectrum at $z = 0$ and the rest-frame FUV spectrum at $z = 1$. This is reflected in the derived IRX – β relation for this combination of filters (Figure A2). Except for the IRX – β relation at $z = 8$ for a MW dust type, all ‘observed’ IRX – β relations based on a photometric sampling are nearly identical to the IRX – β relation based on a direct fit to the rest-frame UV spectrum.

We repeat this exercise for a combination of filters from *GALEX*, a Ks-band filter, HST WFC3 filters, and Subaru filters (this combination is based on the work by Casey et al. 2014). This combination is affected by contamination by the 2175 Å bump at $z = 0$ and $z = 8$ and poorly samples the rest-frame FUV regime of the attenuated stellar spectra of objects at $z = 1$ (Figure A3). These effects lead to a poor reconstruction of the IRX – β relation at $z = 0$ and $z = 8$ for MW and LMC dust types, as well as a poor reconstruction of the IRX – β relation at $z = 1$ for a SMC dust type.

To aid observers, Table A1 lists suggested filter combinations as a function of redshift that reliably reconstruct the UV slope β . To this aim, good photometric coverage of the FUV and the NUV emission is necessary.

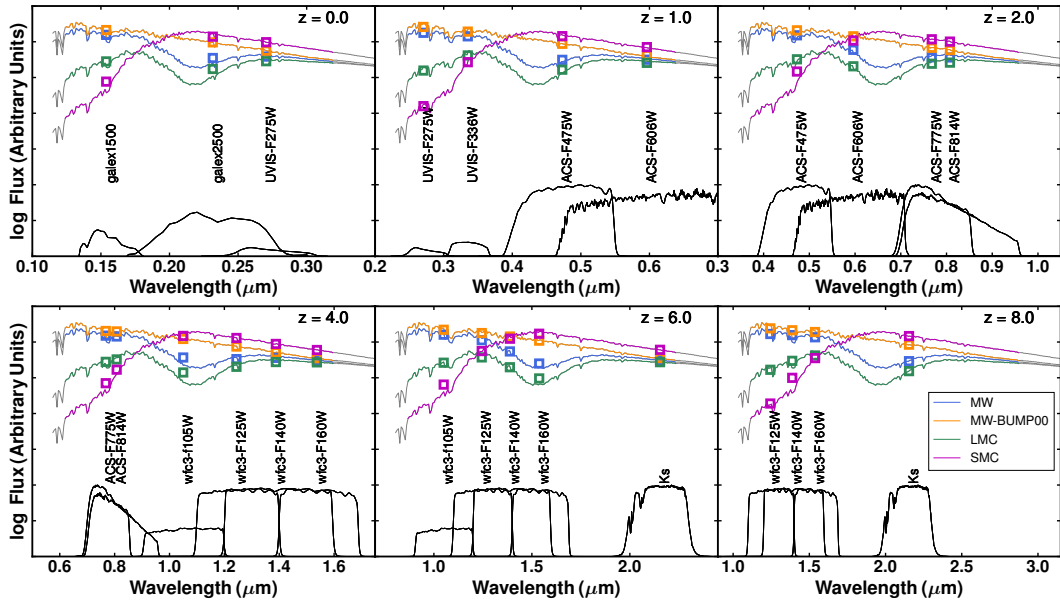


Figure A1. The coverage of the UV rest-frame wavelength regime by different filters for redshifts running from $z = 0$ to $z = 8$, when adopting the four different dust-types in this study. The photometric sampling includes the HST filters that are part of the Reddy et al. (2017) study (3D-HST filters and UVIS-F275W and UVIS-F336W), on top of *GALEX*, and a Ks-band filter. The coloured lines mark the attenuated spectra (from rest-frame 1230 to 3200 Å) assuming a V-band optical depth of $\langle \tau_V \rangle = 1$, whereas the coloured open squares mark the photometric measurements. The relevant filters at each redshift and their transmission curves are plotted below the stellar spectra. The photometric datapoints are marked as coloured squares, where the colours correspond to the attenuated spectra for different dust attenuation curves.

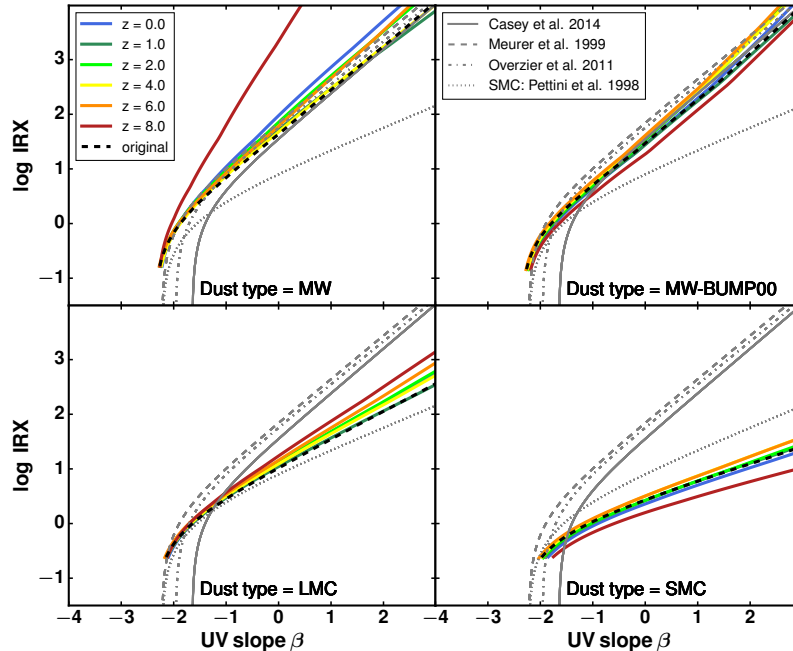


Figure A2. The $IRX - \beta$ relation of stellar emission from different redshifts based on a fit to photometric datapoints for different dust types. The photometric sampling includes the HST filters that are part of the Reddy et al. (2017) study (3D-HST filters and UVIS-F275W and UVIS-F336W), on top of *GALEX*, and a Ks-band filter. Photometric datapoints were obtained by convolving the redshifted stellar spectrum with telescope filters corresponding to the rest-frame wavelength range $1230 < \lambda < 3200$. The black dashed lines correspond to the original $IRX - \beta$ relation derived from a direct fit to the attenuated spectrum. The sampling of telescope filters of the UV wavelength range can completely alter the location of galaxies in the $IRX - \beta$ plane for dust types with a steep UV-slope (SMC dust) or UV absorption features (2175 Å bump; MW and LMC dust). The better sampling of the UV part of the spectrum at e.g., $z = 1$ improves the reconstruction of the $IRX - \beta$ relation.

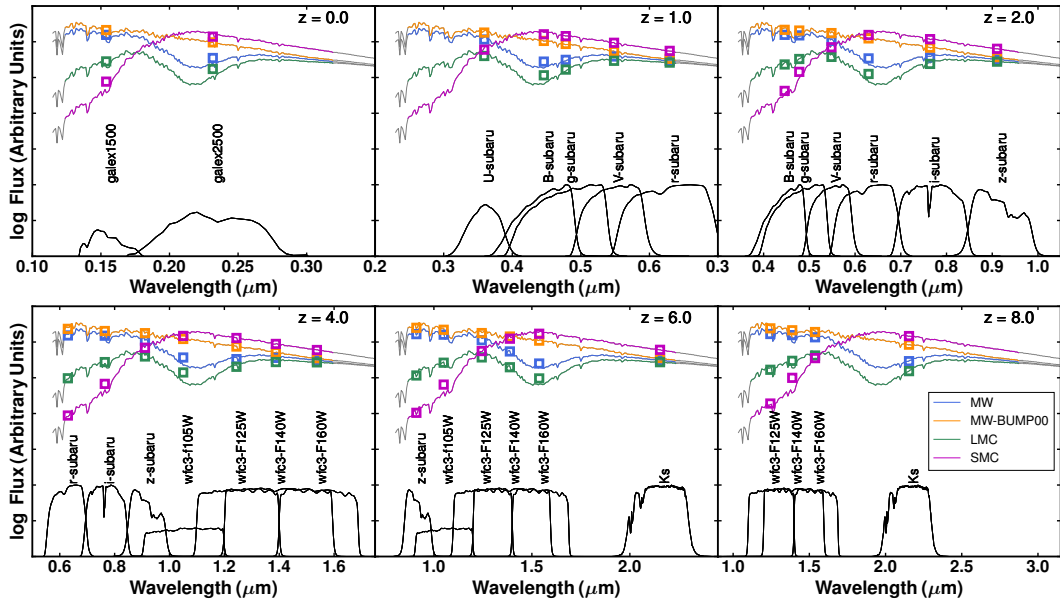


Figure A3. The coverage of the UV rest-frame wavelength regime by different filters for redshifts running from $z = 0$ to $z = 8$, when adopting the four different dust-types in this study. The photometric sampling includes the filters used in Casey et al. (2014, Subaru + HST WFC3), on top of *GALEX*, and a Ks-band filter. The coloured lines mark the attenuated spectra (from rest-frame 1230 to 3200 Å) assuming a V-band optical depth of $\langle \tau_V \rangle = 1$, whereas the coloured open squares mark the photometric measurements. The relevant filters at each redshift and their transmission curves are plotted below the stellar spectra. The photometric datapoints are marked as coloured squares, where the colours correspond to the attenuated spectra for different dust attenuation curves.

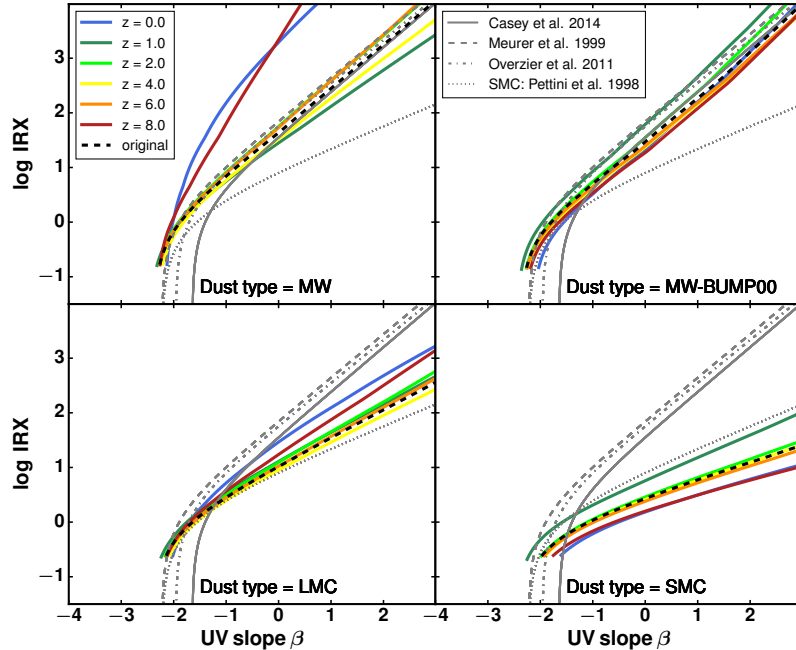


Figure A4. The IRX $-\beta$ relation of stellar emission from different redshifts based on a fit to photometric datapoints for different dust types. The photometric sampling includes the filters used in Casey et al. (2014, Subaru + HST WFC3), on top of *GALEX*, and a Ks-band filter. Photometric datapoints were obtained by convolving the redshifted stellar spectrum with telescope filters corresponding to the rest-frame wavelength range $1230 < \lambda < 3200$. The black dashed lines correspond to the original IRX $-\beta$ relation derived from a direct fit to the attenuated spectrum. The sampling of telescope filters of the UV wavelength range can completely alter the location of galaxies in the IRX $-\beta$ plane for dust types with a steep UV-slope (SMC dust) or UV absorption features (2175 Å bump; MW and LMC dust). The improved sampling of the UV part of the rest-frame spectrum at e.g. $z = 1$ improves the reconstruction of the IRX $-\beta$ relation.

Table A1. A suggestion for combinations of filters (and imaging instruments) for the rest-frame FUV and NUV wavelength range that result in a reliable reconstruction of the UV slope β and the IRX – β relation. Any additional filters with central wavelengths in the rest-frame UV will improve the quality of the reconstruction. Other combinations are of course possible.

redshift	rest-frame FUV wavelengths	rest-frame NUV wavelengths
0.0	<i>GALEX</i> FUV	HST UVIS-F275W
0.5	<i>GALEX</i> NUV	HST ACS-F475W, Subaru B-band, g-band
1.0	HST UVIS-F275W	HST ACS-F606W, Subaru r-band
1.5	HST UVIS-F336W, Subaru U-band	Subaru i-band
2.0	HST ACS-F475W, Subaru B-band, g-band	HST ACS-F814W, Subaru z-band, NIRCam
2.5	HST ACS-F475W, Subaru B-band, g-band	HST WFC3-F105W, MUSE, NIRCam
3.0	HST ACS-F606W, Subaru V-band, NIRCam	HST WFC3-F125W, NIRCam
4.0	HST ACS-F775W, Subaru r-band, NIRCam	HST WFC3-140W, WFC3-160W, NIRCam
5.0	HST ACS-F814W, Subaru i-band, NIRCam	H-band, NIRCam
6.0	HST WFC3-105W, Subaru z-band, NIRCam	Ks-band, NIRCam
7.0	HST WFC3-105W, NIRCam	Ks-band, NIRCam
8.0	HST WFC3-125W, NIRCam	NIRCam